Pure and Applied Functional Analysis
Volume 1, Number 3, 2016, 309–341

Yokohama Publishers
ISSN 2189-3764 ONLINE JOURNAL

FAST COMPUTATION BY SUBDIVISION OF MULTIDIMENSIONAL SPLINES AND THEIR APPLICATIONS

AMIR Z. AVERBUCH, PEKKA NEITTAANMÄKI, GIL SHABAT,
AND VALERY A. ZHELUDEV

Abstract. We present theory and algorithms for fast explicit computations of uni- and multi-dimensional periodic splines of arbitrary order at triadic rational points and of splines of even order at diadic rational points. The algorithms use the forward and the inverse Fast Fourier transform (FFT). The implementation is as fast as FFT computation. The algorithms are based on binary and ternary subdivision of splines. Interpolating and smoothing splines are used for a sample rate convertor such as resolution upsampling of discrete-time signals and digital images and restoration of decimated images that were contaminated by noise. The performance of the rate conversion based spline is compared with the performance of the rate conversion by prolate spheroidal wave functions.

1. Introduction

The goals of the paper are twofold: 1. Design fast algorithms, which provide smooth resolution upsampling of signals/images, that retain the properties of the sampled object. 2. If the signal/image is degraded by noise, the noise is reduced and the structure of the signal/image is revealed. To achieve this, we design interpolating and smoothing splines. Their computational efficiencies are gained by using binary and ternary splines subdivision. The subdivision scheme provides intermediate values for 1D splines. Subdivision schemes are proposed to calculate the splines' values at diadic and triadic rational points.

Splines are important tools in approximation theory, computer aided geometric design and signal/image processing. Splines have been designed by their samples values at grid points. An important problem is how to explicitly design splines of any order and how to achieve a fast calculation of their values at internal points between grid points. In this paper, we propose a fast and efficient scheme for uni- and multi-dimensional periodic splines computations of any order at triadic rational points and of splines of even order at diadic rational points starting from their samples at equidistant grid points. The idea behind the need for having diadic algorithm is the following. The spline $S(t)$, which interpolates available grid samples $S(k)$, is designed and its midpoints values between grid points are explicitly calculated. The

2010 *Mathematics Subject Classification.* 41A15, 65D07, 62D05.
Key words and phrases. Periodic splines, interpolating and smoothing splines, subdivision, rate convertor, restoration, upsampling, prolate spheroidal wave functions.

newly derived samples are interpolated by the new spline whose midpoint values are calculated. Then, this process is iterated. We prove that if the spline order is even then the scheme at each step generates values for the initial spline. Thus, after m iterations, the values $S(k/2^m)$ are derived. The calculations are reduced to the application of a single forward and a single inverse FFT that are independent of the number of iterations. Such a scheme is not valid for odd-order splines. However, a similar subdivision scheme, which utilizes a triadic instead of diadic insertion rule, is applicable to splines of any order. Extension of the algorithms to multidimensional splines is straightforward.

Interpolatory subdivision schemes are refinement rules which iteratively refine data by inserting values that correspond to intermediate points by using linear combinations of values in the initial points, while the data in these initial points are retained.

Restoration and rate conversion to many sample rates such as upsampling (resolution increase) of signals/images are natural applications for these spline algorithms. A spline is designed to interpolate the available samples or pixels. Then, the object's resolution is upsampled by introducing intermediate spline values. If the available data is contaminated by noise then smoothing splines are used for efficient denoising. Performances of upsampling by splines are compared to the performances of the prolate spheroidal wave functions.

There are two common methods for resolution upsampling of signals: One is by zero-padding and the other is by inserting zeros between samples in the Fourier domain of the signal. The application of discrete Fourier transform (DFT) to a zero-padded signal, which becomes an extended signal, inserts complex valued numbers between the interpolated samples. Complex numbers are unsuitable for resolution upsampling. An alternative solution to interpolate the signal is to insert zeros between the signal samples in its Fourier domain and then an interpolating low-pass filter is applied to the extended signa . In fact, this is what is being achieved in the scheme presented in our paper.

In the Fourier domain, inserting zeros between samples is achieved by a doubling (diadic) or tripling (triadic) of the signals in the Fourier domain, followed by the application of the inverse DFT. The algorithm interpolates the signal by inserting zeros between the samples in the Fourier domain and then an interpolating low-pass filter is applied to the extended signal. It is implicitly contained in Eq. (3.13) where in the first line $2N$-point inverse DFT is applied to the N-point DFT of the signal. Low-pas filtering is achieved by multiplication of the signal DFT with the $2N$-periodic sequence. Such filtering results in replacement of the zeros in the intermediate points by values of an even order spline, which interpolates the initial samples. Similar operations are implemented for the ternary upsampling. A practical implementation of the computation of periodic splines at dyadic rational points is described in section 3.4 (Eq. (3.13)) where the detailed implementation algorithm is described by Eq. (3.14). Practical implementation of the computation of periodic splines at triadic rational points is described in section 4.5 (Eq. (4.14)) where the detailed implementation algorithm is described by Eq. (4.15).

The paper is organized as follows. Section 2 provides some preliminaries on interpolatory subdivision and on periodic splines. In particular, design of interpolating

and smoothing splines of any order in one and two dimensions are outlined and their properties are established. In Section 3, the binary subdivision for periodic splines is presented. It leads to periodic splines computation at dyadic rational points and an upsampling algorithm is described. Section 4 does the same for the ternary subdivision schemes. In Section 5, the designed splines are applied to upsampling of signals and images. Applications to restoration from noisy decimated images are also shown.

2. Preliminaries

Throughout the paper, we denote $N = 2^j$, $N_m = 2^m N = 2^{j+m}$, $N_{\tilde{m}} = 3^m N = 2^j\, 3^m$, $j, m \in \mathbb{N}$, $\omega = e^{2\pi i/N}$. The space of N-periodic discrete-time signals is denoted by $\Pi[N]$. The spaces of N_m-periodic and $N_{\tilde{m}}$-periodic signals are denoted as $\Pi[N_m]$ and $\Pi[N_{\tilde{m}}]$, respectively. The forward and inverse discrete Fourier transform (DFT) of signals $\mathbf{x} = \{x[k]\} \in \Pi[N_m]$ and $\tilde{\mathbf{x}} = \{\tilde{x}[k]\} \in \Pi[N_{\tilde{m}}]$ are, respectively,

$$
\begin{aligned}
\hat{x}[n]_m &= \sum_{k=0}^{N_m-1} \omega^{-2^{-m}kn}\, x[k], \quad x[k] = \frac{1}{N_m} \sum_{n=0}^{N_m-1} \omega^{2^{-m}kn}\, \hat{x}[n]_m \\
\hat{\tilde{x}}[n]_{\tilde{m}} &= \sum_{k=0}^{N_{\tilde{m}}-1} \omega^{-3^{-m}kn}\, \tilde{x}[k], \quad \tilde{x}[k] = \frac{1}{N_{\tilde{m}}} \sum_{n=0}^{N_{\tilde{m}}-1} \omega^{3^{-m}kn}\, \hat{\tilde{x}}[n]_{\tilde{m}}.
\end{aligned} \tag{2.1}
$$

For N-periodic signals ($m = 0$), the standard notation is $\hat{x}[n] = \hat{x}[n]_0$.The inner product and the norm in the space $\Pi[N_m]$ are defined as

$$
\begin{aligned}
\langle \mathbf{x}, \mathbf{y} \rangle \stackrel{\Delta}{=} \sum_{k=0}^{N_m-1} x[k]\, y^*[k] &= \frac{1}{N_m} \sum_{n=0}^{N_m-1} \hat{x}[n]_m\, \hat{y}[n]^*_m, \\
\|\mathbf{x}\|^2 \stackrel{\Delta}{=} \sum_{k=0}^{N_m-1} |x[k]|^2 &= \frac{1}{N_m} \sum_{n=0}^{N_m-1} |\hat{x}[n]_m|^2.
\end{aligned}
$$

Similarly, they are defined in the space $\Pi[N_{\tilde{m}}]$. Here, $\cdot^*$ means complex conjugation.

Throughout the paper, $\chi[a, b](t)$ denotes the indicator function of the interval (a, b), which means that $\chi[a, b](t) = 1$ when $t \in (a, b)$ and zero otherwise. The sequence $\delta[k]$ is the Kronecker delta which indicates $\delta[k] = 1$ when $k = 0$ and zero otherwise.

2.1. **Interpolatory subdivision.** Interpolatory subdivision schemes (ISS) are refinement rules, which iteratively refine the data by inserting values that correspond to intermediate points by using linear combinations of values from the initial points while the data in these initial points is preserved. Non-interpolatory schemes update the initial data in addition to the insertion of values into intermediate points.

To be more specific, a univariate subdivision scheme with binary refinement ([10, 11, 25]), denoted by $\mathfrak{S}^2_a$, consists of the following: A function $F(t)$ such that $F(k/2^m) = f^m[k]$, which is defined on the grid $\mathbf{g}^m = \{k/2^m\}_{k\in\mathbb{Z}}$, is extended onto the grid $\mathbf{g}^{m+1}$ by filtering the upsampled array $(\uparrow 2)\mathbf{f}^m = \{\breve{f}^m[k]\}$, ($\breve{f}^m[k] = f^m[l]$, if $k = 2l$, and $\breve{f}^m[k] = 0$, otherwise) by an interpolating filter $\mathbf{a} = \{a[k]\}_{k\in\mathbb{Z}}$ such that $a[2k] = \delta[k]$. Thus, one dyadic refinement step is

$F(k/2^{m+1}) = f^{m+1}[k] = \sum_{l\in\mathbb{Z}} a[k-2l] f^m[l]$, which means that $f^{m+1}[2k] = f^m[k]$ and $f^{m+1}[2k+1] = \sum_{l\in\mathbb{Z}} a[2(k-l)+1] f^m[l]t$. The next refinement step employs $\mathbf{f}^{m+1}$ as an initial data.

A subdivision scheme with ternary refinement ([3, 14, 15]), denoted by $\mathfrak{S}_a^3$, consists of the following: A function $F(t)$ such that $F(k/3^m) = f^m[k]$, which is defined on the grid $\mathbf{g}^m = \{k/3^m\}_{k\in\mathbb{Z}}$, is extended onto the grid $\mathbf{g}^{m+1}$ by filtering the upsampled array $(\uparrow 3)\mathbf{f}^m = \{\breve{f}^m[k]\}$,($\breve{f}^m[k] = f^m[l]$, if $k = 3l$, and $\breve{f}^m[k] = 0$, otherwise) by an interpolating filter $\mathbf{a} = \{a[k]\}_{k\in\mathbb{Z}}$ such that $a[3k] = \delta[k]$. Thus, one triadic refinement step is $F(k/3^{m+1}) = f^{m+1}[k] = \sum_{l\in\mathbb{Z}} a[k-3l] f^m[l]$. It means that $f^{m+1}[3k] = f^m[k]$, and $f^{m+1}[3k\pm 1] = \sum_{l\in\mathbb{Z}} a[3(k-l)\pm 1] f^m[l]t$. The next refinement step employs $\mathbf{f}^{m+1}$ as an initial data.

In this paper, we assume that the initial data array $\mathbf{f}^0$ is N-periodic (belongs to $\Pi[N]$). Consequently, the refined data array $\mathbf{f}^m$ belongs to $\Pi[N_m]$ for the scheme $\mathfrak{S}_a^2$ and belongs to $\Pi[N_{\tilde{m}}]$ for the scheme $\mathfrak{S}_a^3$. In the periodic setting, filtering a signal $\mathbf{x} \in \Pi[N_{\tilde{m}}]$ is interpreted as a discrete circular convolution of the signal with a signal $\mathbf{a}_{\tilde{m}} \in \Pi[N_{\tilde{m}}]$ such that $\mathbf{y} = \mathbf{a}_{\tilde{m}}\,\mathbf{x} \Longleftrightarrow y[k] = \sum_{l=0}^{N_{\tilde{m}}-1} a_{\tilde{m}}[k-l]\, x[l]$. Similarly, it holds for the signals from $\Pi[N_m]$.

2.2. **Space of periodic splines.** Nodes of splines of even and odd orders are located at the points $\{k\}$ and $\{(k+1)/2\}$, $k \in \mathbb{Z}$, respectively.

Definition 2.1. An N-periodic function $S^p(t)$ is called the periodic spline of order $p \in \mathbb{N}$ on the grid $\{k\}$, $k \in \mathbb{Z}$, if it has $p-2$ continuous derivatives (belongs to C^{p-2}) and consists of pieces of polynomials of degree $p-1$ that are linked to each other at the nodes.

The space of N-periodic splines of order p is denoted by ${}^p\mathcal{S}$. A widely used basis for the space ${}^p\mathcal{S}$ consists of shifts of B-splines.

2.2.1. *Periodic B-splines.* Let $N = 2^j$, $j \in \mathbb{N}$. The centered N-periodic B-spline $B^1(t)$ of first order on the grid $\{k\}$, $k \in \mathbb{Z}$, is defined via periodization of the indicator function $\chi[-1/2, 1/2](t)$ of the interval $(-1/2, 1/2)$. That is, $B^1(t) \triangleq \sum_{l\in\mathbb{Z}} \chi[-1/2, 1/2](t + Nl)$.

The Fourier coefficients of the B-spline are

$$c_n(B^1) = \int_{-N/2}^{N/2} B^1(t)\, e^{-2\pi i n t/N} = \int_{-1/2}^{1/2} e^{-2\pi i n t/N} = \frac{\sin \pi n/N}{\pi n/N}.$$

The B-splines of higher order are defined iteratively via the circular convolution $B^p(t) \triangleq B^1 \circledast B^{p-1}(t)$. Thus, B-spline $B^p(t)$ can be expanded into the Fourier series by

$$B^p(t) = \frac{1}{N} \sum_{n\in\mathbb{Z}} e^{2\pi i n t/N} \left(\frac{\sin \pi n/N}{\pi n/N}\right)^p. \tag{2.2}$$

The B-spline $B^p(t)$ is supported on the interval $(-p/2, p/2)$ up to periodization. It is strictly positive inside this interval and symmetric about zero where it has a single maximum. The B-spline B^p consists of pieces of polynomials of degree $p-1$ that

are linked to each other on the nodes such that $B^p \in C^{p-2}$. An explicit expression of the B-spline on the interval $(-N/2, N/2)$ is

$$B^p(t) = \frac{1}{(p-1)!}\sum_{k=0}^{p}(-1)^p \binom{p}{k} \left(t+\frac{p}{2}-k\right)_+^{p-1}, \quad t_+ \triangleq \begin{cases} t, & \text{if } t \geq 0; \\ 0, & \text{otherwise.} \end{cases} \tag{2.3}$$

Certainly, to avoid self-overlapping of the N-periodic B-spline B^p, the inequality $p+1 \leq N$ has to hold.

The integer shifts of the periodic B-spline $\{B^p(t-k)\}$, $k = 0, ..., N-1$, $p \in \mathbb{N}$, form a basis for the space ${}^p\mathcal{S}$. Each spline $S^p(t) \in {}^p\mathcal{S}$ can be represented by

$$S^p(t) = \sum_{k=0}^{N-1} q[k] B^p(t-k), \quad \mathbf{q} = \{q[k]\} \in \Pi[N]. \tag{2.4}$$

The Fourier coefficients of the spline $S^p(t)$ are

$$c_n(S^p) = \int_{-N/2}^{N/2} e^{-2\pi i n t/N} \sum_{k=0}^{N-1} q[k] B^p(t-k)\, dt = \hat{q}[n] \left(\frac{\sin \pi n/N}{\pi n/N}\right)^p. \tag{2.5}$$

2.2.2. *Exponential splines.* The splines

$$\zeta^p[n](t) \triangleq \sum_{k=0}^{N-1} \omega^{kn} B^p(t-k), \quad n = 0, ..., N-1, \tag{2.6}$$

which belong to ${}^p\mathcal{S}$, are called periodic exponential splines. They are the Zak transforms of the periodic B-splines [6, 23].

The application of the inverse DFT (IDFT) to Eq. (2.6) provides a representation for the B-splines via the exponential splines $B^p(t-k) = N^{-1}\sum_{n=0}^{N-1} \zeta^p[n](t)\, \omega^{-kn}$. Substitution of this relation into Eq. (2.4) results in the following spline representation:

$$S^p(t) = \frac{1}{N}\sum_{k=0}^{N-1} q[k] \sum_{n=0}^{N-1} \zeta^p[n](t)\, \omega^{-kn} = \frac{1}{N}\sum_{n=0}^{N-1} \sigma[n]\, \zeta^p[n](t), \quad \sigma[n] \triangleq \hat{q}[n]. \tag{2.7}$$

The N-periodic sequence

$$u^p[n] \triangleq \zeta^p[n](0) = \sum_{k=0}^{N-1} e^{-2\pi i n k/N} B^p(k) \tag{2.8}$$

is called the characteristic sequence of the space ${}^p\mathcal{S}$. Representation of periodic splines by exponential splines, as in Eq. (2.7), generates a variation of harmonic analysis in the spline spaces that is called the spline harmonic analysis (SHA) [2, 4, 24], where the splines $\zeta^p[n](t)$ (Eq. (2.6)) are the counterparts of the Fourier exponentials. We list a few properties of the exponential splines ([2]) that will be used later.

Proposition 2.2. *The following properties of the exponential splines $\zeta^p[n](t) \in {}^p\mathcal{S}$ hold:*

(1) *Expansion into a Fourier series is*

$$\begin{aligned}\zeta^p[n]\,(t) &= \sum_{l\in\mathbb{Z}} e^{2\pi i(n/N+l)t}\,\left(\frac{\sin\pi\,(n/N+l)}{\pi\,(n/N+l)}\right)^p \\ &= \sin^p\frac{\pi n}{N}\sum_{l\in\mathbb{Z}} e^{2\pi i(n/N+l)t}\,\left(\frac{(-1)^l}{\pi\,(n/N+l)}\right)^p.\end{aligned} \tag{2.9}$$

In particular, the characteristic sequence $u^p[n] = \zeta^p[n]\,(0)$ *is represented by*

$$u^p[n] \triangleq \zeta^p[n](0) = \sum_{l\in\mathbb{Z}}\left(\frac{\sin\pi\,(n/N+l)}{\pi\,(n/N+l)}\right)^p = \sin^p\frac{\pi n}{N}\sum_{l\in\mathbb{Z}}\left(\frac{(-1)^l}{\pi\,(n/N+l)}\right)^p. \tag{2.10}$$

(2) *The exponential splines* $\zeta^p[n](t)$ *are the eigenfunctions of the integer shift operator:*

$$\zeta^p[n]\,(t+d) = \omega^{nd}\zeta^p[n](t) \Longrightarrow \zeta^p[n]\,(d) = \omega^{nd}\,u^p[n],\ d\in\mathbb{Z}. \tag{2.11}$$

(3) *The exponential splines* $\zeta^p[n](t)$, $n = 0, \ldots N-1$, *form an orthogonal basis for the space* ${}^p\mathcal{S}$.
(4) *The squared norms of the exponential splines are* $\|\zeta^p[n]\|^2 = N\,u^{2p}[n]$.
(5) *The squared norms of* s $(s < p)$ *derivatives of the exponential splines* $\zeta^p[n](t)$ *are*

$$\left\|(\zeta^p[n])^{(s)}\right\|^2 = N\,\left(2\sin\frac{\pi n}{N}\right)^{2s}\,u^{2(p-s)}[n]. \tag{2.12}$$

Corollary 2.3. *The squared norm of the* s*-th derivative of the spline* $S(t) = N^{-1}\sum_{n=0}^{N-1}\sigma[n]\,\zeta^p[n](t) \in {}^p\mathcal{S}$ *is*

$$\left\|(S^{(s)}\right\|^2 = \frac{1}{N}\sum_{n=0}^{N-1}\left(2\sin\frac{\pi n}{N}\right)^{2s}\,u^{2(p-s)}[n]\,|\sigma[n]|^2. \tag{2.13}$$

Equation (2.8) implies that the characteristic sequence $u^p[n]$ is calculated by the application of DFT to the sampled B-splines. The samples of the B-splines of any order can be calculated by Eq. (2.3).

The B-splines are compactly supported and symmetric about zero. Therefore, the sequences $u^p[n]$ are cosine polynomials $u^p[n] = P_r(\cos\pi n/N)$ of degree $r = [(p+1)/2]$ with real coefficients that have only even-degree terms. The sequences $u^p[n]$ are strictly positive and symmetric about $N/2$.
Examples of characteristic sequences: Denote $y = \cos\pi n/N$. Then

$$u^2[n] = 1, \quad u^3[n] = \frac{1+y^2}{2}, \quad u^4[n] = \frac{1+2y^2}{3}. \tag{2.14}$$

$$u^5[n] = \frac{5+18y^2+y^4}{24}, \quad u^6[n] = \frac{2+11y^2+2y^4}{15}, \tag{2.15}$$

$$u^7[n] = \frac{y^6+179y^4+479y^2+61}{720},\ u^8[n] = \frac{16y^6+4740y^4-4635y^2+1139}{1260}. \tag{2.16}$$

2.3. **Interpolation and smoothing.** A spline, which interpolates a periodic signal $\mathbf{x}$, can be explicitly represented by the basis of exponential splines.

Proposition 2.4. *Any N-periodic signal $\mathbf{x} = \{x[k]\}$, $k \in \mathbb{Z}$, can be uniquely interpolated by a spline $S(k) = x[k]$ from ${}^{p}\mathcal{S}$.*

Proof. f Assume a spline $S^p \in {}^{p}\mathcal{S}$ is expanded by the basis of exponential splines such that
$S^p(t) = N^{-1} \sum_{n=0}^{N-1} \sigma[n]\, \zeta^p[n](t)$. Then, its grid samples are
(2.17)

$$S^p(k) = \frac{1}{N} \sum_{n=0}^{N-1} \sigma[n]\, \zeta^p[n](k) = \frac{1}{N} \sum_{n=0}^{N-1} \sigma[n]\, \omega^{kn}\, \zeta^p[n](0) = \frac{1}{N} \sum_{n=0}^{N-1} \sigma[n]\, \omega^{kn}\, u^p[n].$$

If the spline's values are $S^p(k) = x[k]$ then, by the application of the DFT to both sides of Eq. (2.17), we derive an explicit expression

$$S^p(t) = \frac{1}{N} \sum_{n=0}^{N-1} \frac{\hat{x}[n]}{u^p[n]}\, \zeta^p[n](t) \tag{2.18}$$

for the interpolating spline. □

Definition 2.5. Denote by $\mathcal{F}^r$ the subspace of the $N-$periodic continuous-time signals $f(t)$ that satisfy the condition

$$I(f) \triangleq \int_0^N (f^{(r)}(t))^2\, dt < \infty. \tag{2.19}$$

The subspace of the space $\mathcal{F}^r$, which consists of interpolated discrete-time N-periodic signal $\mathbf{x}$ where $\mathbf{x} = \{x[k]\}$, is denoted by $\mathcal{F}^r_x$.

Splines of even orders from the spaces ${}^{2r}\mathcal{S}$ possess a remarkable property.

Proposition 2.6 ([1,13] Minimal norm property of even-order splines)**.** *The spline $S^{2r}(t) \in {}^{2r}\mathcal{S}$ of even order $2r$, which interpolates the signal $\mathbf{x}$, yields the minimum on the space $\mathcal{F}^r_x$ of the functional $I(f)$ defined in Eq. (2.19) by*

$$S^{2r}(t) = \arg \min_{f \in \mathcal{F}^r_x} \int_0^N (f^{(r)}(t))^2\, dt. \tag{2.20}$$

The claim Proposition 2.6 remains true even when the signal's samples are defined on a non-uniform grid.

2.3.1. *One-dimensional smoothing splines.* Assume that the signal $f(t)$ to be approximated belongs to $\mathcal{F}^r$ and the samples $\mathbf{y} = \{y[k] = f(k) + e_k\}$, $k = 0, ..., N-1$, are given, where $\mathbf{e} = \{e_k\}$ is a vector of random errors that is assumed to be a zero-mean white noise. In addition, assume that the sum $\varepsilon^2 \triangleq \sum_{k=0}^{N-1} e_k^2$ is evaluated. The signal $f(t)$ is approximated by a function $g(t) \in \mathcal{F}^r$, which yields the minimum to the functional I subject to the condition that the discrepancy functional $E_y(g) \triangleq \sum_{k=0}^{N-1} |g(k) - y[k]|^2$ satisfies the condition $E_y(g) \le \varepsilon^2$.

This constrained minimization problem is reduced to the solution of an unconstrained problem: $g_\rho(t) = \arg\min_{g\in\mathcal{F}^r}(J_\rho(g))$, where $J_\rho(g) \stackrel{\Delta}{=} \rho\, I(g) + E_y(g)$, followed by derivation of the optimal value of the numerical parameter ρ from the equation $e(\rho) \stackrel{\Delta}{=} E_y(g_\rho) = \varepsilon^2$.

Proposition 2.7 ([18]). *The unique solution to the minimization problem* $\min_{g\in\mathcal{F}^r} J_\rho(g)$ *is the spline* $S_\rho[\mathbf{y}](t) \in {}^{2r}\mathcal{S}$ *of even order* $2r$.

The spline $S_\rho(t) \in {}^{2r}\mathcal{S}$, which minimizes the functional J_ρ, is called the periodic smoothing spline. The spline $S_\rho(t)$ can be explicitly expressed via the basis of exponential splines. Assume a spline is represented by $S(t) = N^{-1}\sum_{n=0}^{N-1}\sigma[n]\,\zeta^{2r}[n](t)$. Equation (2.13) implies that

$$I(S) = \frac{1}{N}\sum_{n=0}^{N-1}\left(2\sin\frac{\pi n}{N}\right)^{2r} u^{2r}[n]\,|\sigma[n]|^2. \tag{2.21}$$

Due to Eq. (2.17), the grid samples of $S(t)$ are $S(k) = N^{-1}\sum_{n=0}^{N-1}\sigma[n]\,\omega^{kn}\,u^{2r}[n]$. Thus, the the discrepancy functional $E_y(g)$ is expressed by

$$E_y(S) = \frac{1}{N}\sum_{n=0}^{N-1}\left|\sigma[n]\,u^{2r}[n] - \hat{y}[n]\right|^2, \quad \hat{y}[n] = \sum_{k=0}^{N-1}\omega^{-kn}\,y[k]. \tag{2.22}$$

An explicit solution to the unconstrained minimization problem is derived from using Eqs. (2.21) and (2.22). It is the spline from ${}^{2r}\mathcal{S}$ where

$$S_\rho^{2r}(t) = \frac{1}{\sqrt{N}}\sum_{n=0}^{N-1}\sigma[n](\rho)\,\zeta^{2r}[n](t), \quad \sigma[n](\rho) = \frac{\hat{y}[n]}{\rho\,(2\,\sin\pi n/N)^{2r} + u^{2r}[n]}. \tag{2.23}$$

By substituting the coefficients $\sigma[n](\rho)$ into Eq. (2.22), we derive the discrepancy functional for the parameterized spline $S_\rho^{2r}(t)$ to be

$$\begin{aligned} e(\rho) \stackrel{\Delta}{=} E_y(S_\rho) &= \frac{1}{N}\sum_{n=0}^{N-1}\left|\sigma[n](\rho)\,u^{2r}[n] - \hat{y}[n]\right|^2 \\ &= \frac{1}{N}\sum_{n=0}^{N-1}|\hat{y}[n]|^2\left(\frac{\rho\,(2\,\sin\pi n/N)^{2r}}{\rho\,(2\,\sin\pi n/N)^{2r} + u^{2r}[n]}\right)^2. \end{aligned}$$

The function $e(\rho)$ grows monotonically from $e(0) = 0$ to $e(\infty) = N^{-1}\sum_{n=0}^{N-1}|\hat{y}[n]|^2 = \|\mathbf{y}\|^2$. Therefore, the equation

$$e(\rho) = \frac{1}{N}\sum_{n=0}^{N-1}|\hat{y}[n]|^2\left(\frac{\rho\,(2\,\sin\pi n/N)^{2r}}{\rho\,(2\,\sin\pi n/N)^{2r} + u^{2r}[n]}\right)^2 = \varepsilon^2 \tag{2.24}$$

has a unique solution $\bar{\rho}$. The spline $S_{\bar{\rho}}^{2r}(t)$ solves the constrained minimization problem. Its grid samples are

$$S_{\bar{\rho}}^{2r}(k) = \frac{1}{N}\sum_{n=0}^{N-1}\sigma[n](\bar{\rho})\,\omega^{kn}\,u^{2r}[n] = \frac{1}{N}\sum_{n=0}^{N-1}\omega^{kn}\,\frac{\hat{y}[n]\,u^{2r}[n]}{\bar{\rho}\,(2\,\sin\pi n/N)^{2r} + u^{2r}[n]}. \tag{2.25}$$

Equation (2.25) means that the samples $S_{\bar\rho}^{2r}(k)$ are calculated by the application of the IDFT to the sequence $\{\sigma[n](\bar\rho)\}$.

Remark 2.8. The spline $S_{\bar\rho}^{2r}(t)$ can be regarded as a spline that interpolates the signal $\mathbf{s} = \left\{S_{\bar\rho}^{2r}(k)\right\}$. The values between grid points are calculated by the subdivision methods that are described in Sections 3 and 4.

When there are no errors, that is $\varepsilon = 0$, then the parameter is $\bar\rho = 0$ and the grid samples are $S_{\bar 0}^{2r}(k) = y[k] = f(k)$. Thus, the smoothing spline reduces to be an interpolating spline.

2.3.2. *Two-dimensional splines.* The two-dimensional function $S(x,y) \stackrel{\Delta}{=} \sum_{k,n=0}^{N-1} s[k,n]\, B^p(x-k)\, B^q(y-n)$, which is N-periodic in both directions, is a 1D spline of order p with respect to x when the variable y is fixed, and a 1D spline of order q with respect to y when x is fixed. It is called the 2D spline on the grid $\{k,n\}$, $k,n \in \mathbb{Z}$, and the space of such splines is denoted by ${}^{p,q}\mathcal{S}$. An alternative representation of the splines is provided by the exponential splines $S(x,y) = N^{-2}\sum_{\kappa,\nu=0}^{N-1}\sigma[\kappa,\nu]\,\zeta^p[\kappa](x)\,\zeta^q[\nu](y)$. The grid samples of the spline S are

$$S(k,n) = \frac{1}{N^2}\sum_{\kappa,\nu=0}^{N-1} e^{2\pi i(k\kappa+n\nu)}\sigma[\kappa,\nu]\,u^p[\kappa]\,u^q[\nu]. \tag{2.26}$$

Consequently, the spline $S(x,y) \in {}^{p,q}\mathcal{S}$, which interpolates an N-periodic array $\mathbf{z} \stackrel{\Delta}{=} \{z[k,n]\}$ in both directions where $S(k,n) = z[k,n]$, is explicitly represented by

$$\begin{aligned} S(x,y) &= \frac{1}{N^2}\sum_{\kappa,\nu=0}^{N-1}\frac{\hat z[\kappa,\nu]}{u^p[\kappa]\,u^q[\nu]}\,\zeta^p[\kappa](x)\,\zeta^q[\nu](y), \\ \hat z[\kappa,\nu] &\stackrel{\Delta}{=} \sum_{k,n=0}^{N-1} e^{-2\pi i(k\kappa+n\nu)}z[k,n]. \end{aligned} \tag{2.27}$$

The design of two-dimensional smoothing splines is implemented by the same steps as in the 1D design. For simplicity, assume that the splines have the same order in both x and y directions. Assume that the funcion $\varphi(x,y)$ to be approximated is an N-periodic in both directions such that the functional satisfies

$$I(f) \stackrel{\Delta}{=} \int_0^N\int_0^N \left((f_x^{(r)}(x,y))^2 + (f_y^{(r)}(x,y))^2\right) dx\,dy < \infty.$$

Assume that $\mathbf{z} = \{z[k,n] = f(k,n) + e_{k,n}\}, k,n = 0,...,N-1$, where $\mathbf{e} = \{e_{k,n}\}$, $k,n = 0,...,N-1$, is the array of random errors that is a zero-mean white noise. The estimated squared norm of the errors is $\varepsilon^2 = \sum_{k,n=0}^{N-1} e_{k,n}^2$. Denote by $S_\rho(x,y) \in {}^{2r,2r}\mathcal{S}$ the spline that minimizes the parameterized functional $J_\rho(S) \stackrel{\Delta}{=} \rho I(S) + E_z(S)$ on the space ${}^{2r,2r}\mathcal{S}$. The discrepancy functional $E_z(S)$ is defined by $E_z(S) \stackrel{\Delta}{=} \sum_{k,n=0}^{N-1}(S(k,n) - z[k,n])^2$. Equation (2.26) implies that

$$E_z(S) = \frac{1}{N^2}\sum_{\kappa,\nu=0}^{N-1}\left|\sigma[\kappa,\nu]\,u^{2r}[\kappa]\,u^{2r}[\nu] - \hat z[\kappa,\nu]\right|^2. \tag{2.28}$$

The functional becomes

$$I(S) = \frac{1}{N^2} \sum_{\kappa,\nu=0}^{N-1} \left(W^r[\kappa,\nu] + W^r[\nu,\kappa]\right) |\sigma[\kappa,\nu]|^2,$$
$$W^r[\kappa,\nu] \triangleq \left(2 \sin \frac{\pi\kappa}{N}\right)^{2r} u^{2r}[\kappa]\, u^{4r}[\nu]. \tag{2.29}$$

By using Eqs. (2.28) and (2.29), the spline is explicitly represented by

$$S_\rho(x,y) = \frac{1}{N^2} \sum_{\kappa,\nu=0}^{N-1} \sigma[\kappa,\nu](\rho)\, \zeta^{2r}[\kappa](x)\, \zeta^{2r}[\nu](y),$$
$$\sigma[\kappa,\nu](\rho) \triangleq \frac{\hat{z}[\kappa,\nu]\, u^{2r}[\kappa]\, u^{2r}[\nu]}{A^r[\kappa,\nu](\rho)}, \tag{2.30}$$
$$A^r[\kappa,\nu](\rho) \triangleq \rho\left(W^r[\kappa,\nu] + W^r[\nu,\kappa]\right) + (u^{2r}[\kappa]\, u^{2r}[\nu])^2.$$

Like in the 1D case, the value of the regularization parameter ρ is derived from the equation $e(\rho) \triangleq E_z(S_\rho) = \varepsilon^2$ that is expressed by

$$e(\rho) = \frac{1}{N^2} \sum_{\kappa,\nu=0}^{N-1} |\hat{z}[\kappa,\nu]|^2 \left(\frac{(\rho\, (W^r[\kappa,\nu] + W^r[\nu,\kappa])}{A^r[\kappa,\nu](\rho)}\right)^2 = \varepsilon^2, \tag{2.31}$$

Equation (2.31) has a unique solution $\bar{\rho}$. The grid values of the spline $S_{\bar{\rho}}(x,y)$, which is called the 2D smoothing spline, are

$$S_{\bar{\rho}}(k,n) = \frac{1}{N^2} \sum_{\kappa,\nu=0}^{N-1} e^{2\pi i(k\kappa+n\nu)} \frac{\hat{z}[\kappa,\nu]\, (u^{2r}[\kappa]\, u^{2r}[\nu])^2}{\bar{\rho}\left(W^r[\kappa,\nu] + W^r[\nu,\kappa]\right) + (u^{2r}[\kappa]\, u^{2r}[\nu])^2}. \tag{2.32}$$

The grid values are calculated by the application of the 2D IDFT to the sequence $\sigma[\kappa,\nu](\bar{\rho})$. Certainly, when $\varepsilon^2 = 0$, the parameter $\bar{\rho} = 0$ and the spline $S_{\bar{\rho}}(x,y)$ interpolates the initial function $f(x,y)$ such that $S_0(k,n) = f(k,n)$.

3. Binary subdivision for periodic splines

In this section, we present explicit formulae that calculate the values of a spline $S^{2r}(t) \in {}^{2r}\mathcal{S}$ of even order $2r$ at dyadic rational points $\{k/2^m\}$, $k \in \mathbb{Z}$, $m \in \mathbb{N}$, where its samples on the grid $\mathbf{g} = \{k\}$, $k \in \mathbb{Z}$, are $S(k) = y[k]$. In this case, the utilization of exponential splines makes the spline computations of arbitrary even orders straightforward.

3.1. **Spline spaces with different dyadic resolution scales.** We have dealt so far with splines from the spaces ${}^p\mathcal{S}$ whose nodes are located on the grid $\{k\}$. In this section, we introduce an embedded set of periodic splines' spaces that correspond to different dyadic resolution scales.

We recall the notations: $N = 2^j$, $N_m = 2^m N = 2^{j+m}$, $j, m \in \mathbb{N}$ and $\omega \triangleq e^{2\pi i/N}$. Denote by ${}^p\mathcal{S}_m$ the space of $N-$periodic splines of order p on the grid $\{k/2^m\}$. The notation ${}^p\mathcal{S}$ is reserved for the space ${}^p\mathcal{S}_0$. Obviously, the space ${}^p\mathcal{S}_m$ is a subspace of ${}^p\mathcal{S}_{m+1}$. Thus, we get a set of periodic splines' spaces that correspond to different resolution scales such that ${}^p\mathcal{S} \subset {}^p\mathcal{S}_1 .... \subset {}^p\mathcal{S}_m ...$.

Denote $\beta_m^1(t) \triangleq 2^m\,\chi(-2^{-m-1}, 2^{-m-1})$, where $\chi[a,b](t)$ is the indicator function. The N-periodic normalized B-spline of the first order on the grid $\{2^{-m}\,k\}$ and its Fourier coefficients are

$$B_m^1(t) \triangleq \sum_{k\in\mathbb{Z}} \beta_m^1\left(t+kN\right), \quad c_n(B_m^1) = \frac{\sin \pi n/N_m}{\pi n/N_m}.$$

The N-periodic normalized B-spline of order p, which is defined via the iterated circular convolution, is

$$B_m^p(t) \triangleq B_m^1 \circledast B_m^{p-1}(t) = \frac{1}{N}\sum_{n\in\mathbb{Z}} \left(\frac{\sin(\pi n/N_m)}{\pi n/N_m}\right)^p e^{2\pi i n t/N}. \tag{3.1}$$

Each spline $S_m(t) \in {}^p\mathcal{S}_m$ is represented by

$$S_m(t) = \sum_{k=0}^{N_m-1} q[k]\,B_m^p\left(t-2^{-m}k\right) = \frac{1}{N_m}\sum_{n=0}^{N_m-1} \xi[n]\,\zeta_m^p[n](t), \quad \xi[n] = \hat{q}[n]_m, \tag{3.2}$$

where the exponential splines, which form orthogonal bases of ${}^p\mathcal{S}_m$, are the Zak transforms of the B-splines given for $n = 0, ..., N_m - 1$, by

$$\zeta_m^p[n](t) \triangleq \sum_{k=0}^{N_m-1} \omega^{2^{-m}nk} B_m^p(t-2^{-m}k) = 2^m \sum_{l\in\mathbb{Z}} e^{2\pi i(n/N+2^m l)t} \left(\frac{\sin \pi(n/N_m+l)}{\pi(n/N_m+l)}\right)^p. \tag{3.3}$$

The N_m-periodic characteristic sequence of the space ${}^p\mathcal{S}_m$ is

$$u_m^p[n] \triangleq \zeta_m^p[n](0) = \sum_{k=0}^{N_m-1} \omega^{-2^{-m}nk} B_m^p(2^{-m}k) = 2^m \sum_{l\in\mathbb{Z}} \left(\frac{\sin \pi(n/N_m+l)}{\pi(n/N_m+l)}\right)^p. \tag{3.4}$$

The spline $S_m(t) \in {}^p\mathcal{S}_m$, which interpolates an N_m-periodic signal $\mathbf{x} = \{x[k]\}$ by $S(2^{-m}\,k) = x[k],\ k \in \mathbb{Z}$, is

$$S_m(t) = \frac{1}{N_m}\sum_{n=0}^{N_m-1} \frac{\hat{x}[n]_m}{u_m^p[n]}\,\zeta_m^p[n](t), \quad \hat{x}[n]_m = \sum_{k=0}^{N_m-1} \omega^{-2^{-m}nk} x[k]. \tag{3.5}$$

Proposition 3.1. *The characteristic sequence $u_m^p[n]$ of the space ${}^p\mathcal{S}_m$ is calculated by the application of the $2^m N-$point DFT to the sampled B-spline $B^p(t) \in {}^p\mathcal{S}$.*

Proof. Replace N by $N_m = 2^m N$ in Eqs. (2.8) and (2.10), and compare the result with Eq. (3.4). We get

$$\sum_{k=0}^{N_m-1} e^{-2\pi i n k/N_m} B^p(k) = \sum_{l\in\mathbb{Z}} \left(\frac{\sin \pi\left(n/N_m+l\right)}{\pi\left(n/N_m+l\right)}\right)^p = 2^{-m}\,u_m^p[n].$$

Thus, the sequence $u_m^p[n]$ is the output from the application of the $2^m N-$point DFT to the sampled B-spline $\left\{b^p[k] \triangleq B^p(k)\right\}$ multiplied by 2^m to become $u_m^p[n] = 2^m\,\hat{b}^p[n]_m = 2^m\,\sum_{k=0}^{N_m-1} \omega^{-2^{-m}kn}\,B^p(k)$. □

Remark 3.2. The previous notation $\zeta^p[n](t) \equiv \zeta_0^p[n](t)$, $u^p[n] \equiv u_0^p[n]$, are reserved for splines on the initial scale $m = 0$.

3.2. **Insertion rule.** Calculation of the values of even-order splines at dyadic rational points is based on the following insertion rule:

Dyadic periodic spline insertion rule: *Assume that* $\mathbf{f}^0 \triangleq \left\{f^0[k]\right\}$, $k \in \mathbb{Z}$, *is an* N*-periodic sequence. For* $m = 1, 2, \ldots$, *we construct a spline* $S_{m-1}(t) \in {}^p\mathcal{S}_{m-1}$ *on the grid* $\mathbf{g}^{m-1} \triangleq \left\{k/2^{m-1}\right\}$, $k \in \mathbb{Z}$, *such that* $S_{m-1}\left(k/2^{m-1}\right) = f^{m-1}[k]$, $k \in \mathbb{Z}$. *Then,* $f^m[k] \triangleq S_{m-1}\left(k/2^m\right)$, $k \in \mathbb{Z}$.

In other words, in order to refine the data $\mathbf{f}^{m-1}$ from the grid $\left\{k/2^{m-1}\right\}$ to the grid $\{k/2^m\}$, we construct the spline $S_{m-1}(t)$, which interpolates $\mathbf{f}^{m-1}$ on the grid $\left\{k/2^{m-1}\right\}$ and define $f^m[2k] \triangleq f^{m-1}[k]$, $\quad f^m[2k+1] \triangleq S_{m-1}((k+1/2)\,2^{m-1})$, that are the spline values at midpoints between the interpolation points.

If the spline's order is even then this insertion rule reproduces the spline, which means that $S_m(t) \equiv S_{m-1}(t) \equiv \ldots \equiv S_0(t)$. Consequently, each refinement step provides the spline's $S_0(t)$ values at the subsequent set of dyadic rational points.

Theorem 3.3. *Let* $S(t) \in {}^{2r}\mathcal{S}$ *be an* N*-periodic spline of order* $2r$ *with nodes on the grid* $\{k\}$, $k \in \mathbb{Z}$. *Its samples are* $\left\{S(k) = f^0[k]\right\}$, $\mathbf{f}^0 \triangleq \left\{f^0[k]\right\}$, $k \in \mathbb{Z}$. *Then, all the subsequent subdivision steps with the dyadic spline insertion rule reproduce the values* $\left\{f^m[k] = S(k/2^m)\right\}$, $k \in \mathbb{Z}$, $m = 1, 2, \ldots$ *of this spline.*

Proof. Due to the minimal norm property (Proposition 2.6), we get

$$\mu \triangleq \int_0^N |S^{(r)}(t)|^2\,dt \le \int_0^N |g^{(r)}(t)|^2\,dt,$$

where $g(t)$ is any function such that $g^{(r)}(t)$ is a square integrable and $\left\{g(k) = f^0[k]\right\}$, $k \in \mathbb{Z}$. Let $S_1(t) \in {}^{2r}\mathcal{S}_1$ be a spline of order $2r$ that interpolates the values $\{f^1[k] = S(k/2)\}_{k\in\mathbb{Z}}$. Then,

$$\nu \triangleq \int_0^N |S_1^{(r)}(t)|^2\,dt \le \int_0^N |G^{(r)}(t)|^2\,dt,$$

where $G(t)$ is any function such that $G^{(r)}(t)$ is square integrable and $G(k/2) = f^1[k] = S(k/2)$. Hence, $\nu \le \mu$. On the other hand, $S_1(k) = f^0[k]$, therefore, $\mu \le \nu$. Thus, $\int_0^N |S^{(r)}(t)|^2\,dt = \int_0^N |S_1^{(r)}(t)|^2\,dt$. Hence, it follows that $S_1(t) \equiv S(t)$. Repeating the above reasoning, we get that the spline $S_2(t) \in {}^{2r}\mathcal{S}_2$, which interpolates the values $\{f^2[k] = S_1(k/4)\}_{k\in\mathbb{Z}}$, coincides with $S_1(t)$. Consequently, it coincides with $S(t)$. The same is true for any spline $S_m(t) \in {}^{2r}\mathcal{S}_{2^m}$ that interpolates the values $\{f^m[k] = S_{m-1}(k/2^m)\}_{k\in\mathbb{Z}}$. □

3.3. **Periodic spline filters for binary subdivision.** The spline $S_0(t) \in {}^p\mathcal{S}$, which interpolates an N-periodic sequence $\mathbf{f}^0 \triangleq \left\{f^0[k]\right\}$ such that $S(k) = f^0[k]$, $k \in \mathbb{Z}$, is represented by

$$S_0(t) = \frac{1}{N}\sum_{n=0}^{N-1} \frac{\hat{f}^0[n]}{u^p[n]}\,\zeta^p[n](t), \quad \hat{f}^0[n] = \sum_{k\in\mathbb{Z}} \omega^{-kn} f^0[k], \tag{3.6}$$

where $\zeta^p[n](t)$ are the exponential splines defined in Eq. (2.6) whose Fourier expansion is given in Eq. (2.9). The characteristic sequence $u^p[n] = \zeta^p[n](0)$ of the space ${}^p\mathcal{S}$ is presented by Eq. (2.8).

The DFT of the refined array is split into the polyphase components

$$\begin{aligned}\hat{f}^1[n]_1 &= \sum_{k=0}^{2N-1} \omega^{-kn/2}\, f^1[k] = \hat{f}_0^1[n] + \omega^{-n/2}\hat{f}_1^1[n],\\ \hat{f}_0^1[n] &\triangleq \sum_{k=0}^{N-1} \omega^{-kn}\, f^1[2k] = \hat{f}^0[n], \quad \hat{f}_1^1[n] \triangleq \sum_{k=0}^{N-1} \omega^{-kn}\, f^1[2k+1].\end{aligned} \tag{3.7}$$

According to the dyadic insertion rule and the shift property (Eq. (2.11)) of the exponential splines, we get $f^1[2k+1] = S_0\,(k+1/2)$ and

$$\begin{aligned}S_0\left(k+\frac{1}{2}\right) &= \frac{1}{N}\sum_{n=0}^{N-1} \frac{\hat{f}^0[n]}{u^p[n]}\,\zeta^p[n]\left(k+\frac{1}{2}\right),\\ \zeta^p[n]\left(k+\frac{1}{2}\right) &= \omega^{kn}\,\omega^{n/2}\,\upsilon^p[n]\\ \upsilon^p[n] &\triangleq \omega^{-n/2}\,\zeta^p[n]\left(\frac{1}{2}\right) = \sum_{l\in\mathbb{Z}} e^{\pi i l}\,\left(\frac{\sin\pi\,(n/N+l)}{\pi\,(n/N+l)}\right)^p.\end{aligned} \tag{3.8}$$

Consequently,

$$f^1[2k+1] = \frac{1}{N}\sum_{n=0}^{N-1} \frac{\hat{f}^0[n]}{u^p[n]}\,\omega^{kn}\,\omega^{n/2}\,\upsilon^p[n] \Longrightarrow \hat{f}_1^1[n] = \omega^{n/2}\frac{\upsilon^p[n]}{u^p[n]}\,\hat{f}^0[n]. \tag{3.9}$$

By substituting Eq. (3.9) into Eq. (3.7), we get

$$\hat{f}^1[n]_1 = \hat{a}_0^p[n]\,\hat{f}^0[n] \Longleftrightarrow f^1[k] = \frac{1}{2N}\sum_{k=0}^{2N-1} \omega^{kn/2}\,\hat{a}_0^p[n]\,\hat{f}^0[n], \tag{3.10}$$

$$\text{where } \hat{a}_0^p[n] \triangleq \frac{u^p[n]+\upsilon^p[n]}{u^p[n]}.$$

Thus, the refined sequence $\mathbf{f}^1$ is derived by filtering the initial data $\mathbf{f}^0$ with the filter $\mathbf{a}_0^p$, whose frequency response $\hat{a}_0^p[n]$ is defined in Eq. (3.10).

Proposition 3.4. *If the order is $p = 2r$ then the frequency response of the filter $\mathbf{a}_0^p$ is*

$$\hat{a}_0^{2r}[n] = 2\,\cos^{2r}\frac{\pi n}{2N}\,\frac{u_1^{2r}[n]}{u^{2r}[n]}, \quad n = 0, ..., 2N-1, \tag{3.11}$$

where the sequence $u_1^{2r}[n]$ is defined in Eq. (3.4).

Proof. Denote $A[n] \triangleq u^{2r}[n] + \upsilon^{2r}[n]$. Then, $\hat{a}_0^{2r}[n] = A[n]/u^{2r}[n]$. By combining Eqs (2.8) and (3.8) we get

$$A[n] = \sum_{l\in\mathbb{Z}} \left(1+e^{i\pi l}\right)\left(\frac{\sin\pi\,(n/N+l)}{\pi\,(n/N+l)}\right)^{2r} = \sum_{l\in\mathbb{Z}} \left(1+(-1^l)\right)\left(\frac{\sin\pi\,(n/N+l)}{\pi\,(n/N+l)}\right)^{2r}.$$

Thus, only the even terms in the series remain

$$\begin{aligned} A[n] &= 2\sum_{l\in\mathbb{Z}}\left(\frac{\sin 2\pi\,(n/2N+l)}{2\pi\,(n/2N+l)}\right)^{2r} \\ &= 2\sum_{l\in\mathbb{Z}}\left(\frac{\sin\pi\,(n/2N+l)\,\cos\pi\,(n/2N+l)}{\pi\,(n/2N+l)}\right)^{2r} \\ &= 2\cos^{2r}\frac{\pi n}{2N}\sum_{l\in\mathbb{Z}}\left(\frac{\sin\pi\,(n/2N+l)}{\pi\,(n/2N+l)}\right)^{2r} = 2\cos^{2r}\frac{\pi n}{2N}\;u_1^{2r}[n]. \end{aligned}$$

□

Similarly to Eq. (3.10), we obtain an expression for the refinement from resolution scale $m-1$:

$$\hat{f}^m[n]_m = \hat{a}_{m-1}^{2r}[n]\,\hat{f}^{m-1}[n]_{m-1},\quad \hat{a}_{m-1}^{2r}[n] = 2\,\cos^{2r}\frac{\pi n}{N_m}\,\frac{u_m^{2r}[n]}{u_{m-1}^{2r}[n]}, \tag{3.12}$$

where $u_m^{2r}[n]$ are defined in Eq. (3.4) and $n = 0, ..., N_m - 1$.

3.4. **Computation of periodic splines at dyadic rational points: Practical implementation.** Assume that the samples $\left\{S(k) = f^0[k]\right\}$, $k = 0, ..., N-1$, of a spline $S(t) \in {}^{2r}\mathcal{S}$ are given. It follows from Eq. (3.12) that its values $\{S(k/2^m)\}$, $k \in \mathbb{Z}$, are derived by the application of m successive refinement steps with the initial data $\mathbf{f}^0$ and the filters $\mathbf{a}_0^{2r}$, $\mathbf{a}_1^{2r}$,...,$\mathbf{a}_{m-1}^{2r}$, whose frequency responses are given in Eq. (3.12). This process can be described explicitly. From Eq. (3.12), we get

$$\begin{aligned} \hat{f}^1[n]_1 &= \hat{a}_0^{2r}[n]\,\hat{f}^0[n],\quad \hat{a}_0^{2r}[n] = 2\cos^{2r}\frac{\pi n}{2N}\,\frac{u_1^{2r}[n]}{u^{2r}[n]}\,\hat{f}^0[n], \\ \hat{f}^2[n]_2 &= 2\,\cos^{2r}\frac{\pi n}{4N}\,\frac{u_2^{2r}[n]}{u_1^{2r}[n]}\hat{f}^1[n]_1 \\ &= 2^2\cos^{2r}\frac{\pi n}{4N}\;\cos^{2r}\frac{\pi n}{2N}\,\frac{u_2^{2r}[n]\,u_1^{2r}[n]}{u_1^{2r}[n]\,u^{2r}[n]}\hat{f}^0[n], \\ &\cdots \\ \hat{f}^m[n]_m &= 2^m\,\frac{u_m^{2r}[n]}{u^{2r}[n]}\hat{f}^0[n]\,\prod_{l=1}^{m}\cos^{2r}\frac{\pi n}{2^l N}. \end{aligned} \tag{3.13}$$

Computation of the values $S(k/2^m) = f^m[k]$ of the spline $S(t) \in {}^{2r}\mathcal{S}$ from the samples $S(k) = f^0[k]$ is reduced to the following three steps:

(1) Apply the $N-$point DFT to the initial data $\mathbf{f}^0 = \left\{f^0[k]\right\}$ to get $\hat{f}^0[n] = \sum_{k=0}^{N-1}\omega^{-kn}f^0[k]$.
(2) Multiply the array $\left\{f^0[n]\right\}$ by

$$\hat{f}^m[n]_m = 2^m\,\frac{u_m^{2r}[n]}{u^{2r}[n]}\,\hat{f}^0[n]\,\prod_{l=1}^{m}\cos^{2r}\frac{\pi n}{2^l N}$$

where $u^{2r}[n]$ and $\hat{f}^0[n]$ are $N-$periodic sequences, while $u_m^{2r}[n]$ is $2^m N-$periodic.

(3) Apply the $2^m N-$point IDFT to the sequence $\hat{\mathbf{f}}^m = \left\{\hat{f}^m[n]_m\right\}$ to get

$$S(k/2^m) = f^m[k] = \frac{1}{N_m}\sum_{n=0}^{N_m-1}\omega^{-2^m kn}\,\hat{f}^m[n]_m. \tag{3.14}$$

The above algorithm interpolates the signal by inserting zeros between the samples in the Fourier domain and then apply to the extended signal an interpolating low-pass filter. It is implicitly contained in Eq. 3.13 where in the first line $2N$-point inverse DFT is applied to the N-point DFT of the signal f such that $\hat{f}^0[n]$. Low-pas filtering is achieved by multiplication of the DFT of the signal f by the $2N$-periodic sequence $2\cos^{2r}\frac{\pi n}{2N}\frac{u_1^{2r}[n]}{u^{2r}[n]}$. Such filtering results in replacement of the zeros in the intermediate points by values of the $2r$-order spline, which interpolates the initial samples. Similar operations are implemented for the ternary upsampling shown in section 4.

4. Ternary periodic subdivision

Section 3.4 established that the values of even-order splines at the dyadic rational points can be derived from the initial grid samples by Eq. (3.14). This is not the case for splines of odd order. The above binary subdivision scheme, being applied to an odd-order spline, does not restore this spline but rather converges to a function that is smoother than the original spline ([25]). However, the ternary subdivision scheme in Section 4.1 restores the values of the spline of any order at the triadic rational points $\{3^{-m}k\}\,,\ m\in\mathbb{N}$.

4.1. Super-resolution spline spaces (triadic scale).

In this section, $N=2^j,\ j\in\mathbb{N}$, $\tilde{N}_m = 3^m N,\ m=1,2,...,$ and $\omega \triangleq e^{2\pi i/N}$. The "triadic" DFT of an $\tilde{N}_m-$periodic signal $\mathbf{x}=\{x[k]\}$ is defined in Eq. (2.1).

We refine the spline space ${}^p\mathcal{S}$ along the triadic scale ${}^p\mathcal{S} = {}^p\tilde{\mathcal{S}}_0 \subset {}^p\tilde{\mathcal{S}}_1 \subset {}^p\tilde{\mathcal{S}}_2... \subset {}^p\tilde{\mathcal{S}}_m...$, where ${}^p\tilde{\mathcal{S}}_m$ denotes the space of $N-$periodic splines of order p defined on the grid $\{3^{-m}\,k\}\,,\ k\in\mathbb{Z},\ m=0,1,\ldots$.

The N-periodic normalized B-spline of the first order on the grid $\{3^{-m}\,k\}$ and its Fourier coefficients are

$$\tilde{B}_m^1(t) \triangleq \sum_{k\in\mathbb{Z}} 3^m \chi[-3^{-m-1},3^{-m-1}]\,(t+kN)\,,\quad c_n(\tilde{B}_m^1) = \frac{\sin \pi n/\tilde{N}_m}{\pi n/\tilde{N}_m},$$

where $\chi[a,b](t)$ is the indicator function.

The N-periodic triadic normalized B-spline of order p is defined via the iterated circular convolution

$$\tilde{B}_m^p(t) \triangleq \tilde{B}_m^1 \circledast \tilde{B}_m^{p-1}(t) = \frac{1}{N}\sum_{n\in\mathbb{Z}}\left(\frac{\sin(\pi n/\tilde{N}_m)}{\pi n/\tilde{N}_m}\right)^p e^{2\pi i n t/N}.$$

Each spline $S(t)\in {}^p\tilde{\mathcal{S}}_m$ is represented by

$$S(t) \;=\; \sum_{k=0}^{\tilde{N}_m-1} q[k]\tilde{B}_m^p\left(t-3^{-m}k\right) = \frac{1}{\tilde{N}_m}\sum_{n=0}^{\tilde{N}_m-1}\xi[n]\,\tilde{\zeta}_m^p[n](t),$$

$$\xi[n] \;=\; \sum_{k=0}^{\tilde{N}_m-1} e^{-2\pi i n k/\tilde{N}_m} q[k],$$

where the exponential splines, which form the orthogonal bases of ${}^p\tilde{\mathcal{S}}_m$, are

$$\begin{aligned}\tilde{\zeta}_m^p[n](t) &\triangleq \sum_{k=0}^{\tilde{N}_m-1} e^{2\pi i n k/\tilde{N}_m} \tilde{B}_m^p(t-3^{-m}k) \\ &= 3^m \sum_{l\in\mathbb{Z}} e^{2\pi i(n/N+3^m l)t} \left(\frac{\sin\pi(n/\tilde{N}_m+l)}{\pi(n/\tilde{N}_m+l)}\right)^p,\end{aligned}$$

$n = 0, ..., \tilde{N}_m - 1$. The $\tilde{N}_m$ -periodic characteristic sequence of the space ${}^p\tilde{\mathcal{S}}_m$ is (4.1)

$$\tilde{u}_m^p[n] \triangleq \tilde{\zeta}_m^p[n](0) = \sum_{k=0}^{\tilde{N}_m-1} e^{2\pi i n k/\tilde{N}_m} \tilde{B}_m^p(3^{-m}k) = 3^m \sum_{l\in\mathbb{Z}} \left(\frac{\sin\pi(n/\tilde{N}_m+l)}{\pi(n/\tilde{N}_m+l)}\right)^p.$$

The proof Proposition 4.1 is similar to the proof of Proposition 3.1.

Proposition 4.1. *The characteristic sequence $\tilde{u}_m^p[n]$ of the space ${}^p\tilde{\mathcal{S}}_m$ is calculated by the application of $3^m N-$point DFT to the sampled B-spline $B^p(t) \in {}^p\mathcal{S}$ such that*

$$\tilde{u}_m^p[n] = 3^m\, \hat{b}^p[n]_{\tilde{m}} = 3^m \sum_{k=0}^{\tilde{N}_m-1} \omega^{-3^{-m}kn}\, B^p(k).$$

The spline $S(t) \in {}^p\tilde{\mathcal{S}}_m$, which interpolates an $\tilde{N}_m$ -periodic signal $\mathbf{x} = \{x[k]\}$, is $S(k/3^m) = x[k],\ k \in \mathbb{Z}$ such that

$$S(t) = \frac{1}{\tilde{N}_m} \sum_{n=0}^{\tilde{N}_m-1} \frac{\hat{x}[n]_{\tilde{m}}}{\tilde{u}_m^p[n]}\, \tilde{\zeta}_m^p[n](t), \quad \hat{x}[n]_{\tilde{m}} \triangleq \sum_{k=0}^{\tilde{N}_m-1} \omega^{-3^{-m}nk} x[k].$$

4.2. **Insertion rule.** Calculation of the N-periodic splines of order p at triadic rational points is based on the following insertion rule:

Triadic periodic spline insertion rule: *Assume that $\mathbf{f}^0 \triangleq \left\{f^0[k]\right\},\ k \in \mathbb{Z}$, is an N-periodic sequence. For $m = 1, 2, \ldots$, we construct a spline $S_{m-1}(t) \in {}^p\tilde{\mathcal{S}}_{m-1}$, on the grid $\tilde{\mathbf{g}}^{m-1} \triangleq \left\{k/3^{m-1}\right\},\ k \in \mathbb{Z}$, such that $S_{m-1}\left(k/3^{m-1}\right) = f^{m-1}[k],\ k \in \mathbb{Z}$. Then, $f^m[k] \triangleq S_{m-1}\left(k/3^m\right),\ k \in \mathbb{Z}$.*

In other words, in order to refine the data $\mathbf{f}^{m-1}$ from the grid $\left\{k/3^{m-1}\right\}$ to the grid $\{k/3^m\}$, we construct the spline $S_{m-1}(t)$, which interpolates $\mathbf{f}^{m-1}$ on the grid $\left\{k/3^{m-1}\right\}$ and define $f^m[3k] = f^{m-1}[k]$ and $f^m[3k \pm 1] = S_{m-1}((k \pm 1/3)/3^{m-1})$, that are the spline values at points around the interpolation points.

This insertion rule reproduces a spline of any order, which means that $S_m(t) \equiv S_{m-1}(t) \equiv ... \equiv S_0(t)$. Consequently, each refinement step provides the values of the spline $S_0(t)$ at a subsequent set of triadic rational points. The proof of this fact for splines of arbitrary order is given in Section 4.4.

4.3. **Periodic spline filters for ternary subdivision.** The spline $S_0(t) \in {}^p\mathcal{S}$, which interpolates the N-periodic sequence $\mathbf{f}^0 \triangleq \{f^0[k]\}$ $(S(k) = f^0[k],\ k \in \mathbb{Z})$, is represented by

$$S_0(t) = \frac{1}{N}\sum_{n=0}^{N-1} \frac{\hat{f}^0[n]}{u^p[n]}\,\zeta^p[n](t), \quad \zeta^p[n](t) = \sum_{l\in\mathbb{Z}} e^{2\pi i(n/N+l)t}\left(\frac{\sin\pi\,(n/N+l)}{\pi\,(n/N+l)}\right)^p.$$

The DFT of the refined array is

(4.2)

$$\begin{aligned} \hat{f}^1[n]_{\tilde{1}} &= \hat{f}^1_0[n] + e^{-2\pi in/3N}\hat{f}^1_1[n] + e^{2\pi in/3N}\hat{f}^1_{-1}[n], \\ \hat{f}^1_0[n] &\triangleq \textstyle\sum_{k=0}^{N-1}\omega^{-kn} f^1[3k] = \hat{f}^0[n], \quad \hat{f}^1_{\pm1}[n] \triangleq \sum_{k=0}^{N-1}\omega^{-kn} f^1[3k\pm1]. \end{aligned}$$

According to the triadic insertion rule and the shift property (Eq. (2.11)) of the splines $\zeta^p[n](t)$, we get

$$f^1[3k\pm1] = S_0\left(k\pm\frac{1}{3}\right) = \frac{1}{N}\sum_{n=0}^{N-1}\frac{\hat{f}^0[n]}{u^p[n]}\,\zeta^p[n]\left(k\pm\frac{1}{3}\right)$$

$$\zeta^p[n]\left(k\pm\frac{1}{3}\right) = \omega^{kn}\,e^{\pm2\pi in/3N}\,\upsilon^p_{\pm1}[n], \qquad \text{where}$$

$$\upsilon^p_{\pm1}[n] \triangleq e^{\mp2\pi in/3N}\,\zeta^p[n]\left(\frac{1}{3}\right) = \sum_{l\in\mathbb{Z}} e^{\pm2\pi il/3}\left(\frac{\sin\pi\,(n/N+l)}{\pi\,(n/N+l)}\right)^p. \tag{4.3}$$

Consequently,

(4.4)

$$f^1[3k\pm1] = \frac{1}{N}\sum_{n=0}^{N-1}\frac{\hat{f}^0[n]}{u^p[n]}\,\omega^{kn}\,e^{\pm2\pi in/3N}\,\upsilon^p_{\pm1}[n] \Longrightarrow \hat{f}^1_{\pm1}[n] = e^{\pm2\pi in/3N}\frac{\upsilon^p_{\pm1}[n]}{u^p[n]}\,\hat{f}^0[n].$$

By substituting Eqs. (4.3) and (4.4) into Eq. (4.2), we get

$$\hat{f}^1[n]_{\tilde{1}} = \hat{a}^p_0[n]\,\hat{f}^0[n], \quad f^1[k] = \frac{1}{3N}\sum_{k=0}^{3N-1}\omega^{kn/3}\,\hat{a}^p_0[n]\,\hat{f}^0[n], \tag{4.5}$$

$$\text{where } \hat{a}^p_0[n] \triangleq \frac{u^p[n] + \upsilon^p_1[n] + \upsilon^p_{-1}[n]}{u^p[n]}.$$

Equation (4.5) means that the refined array $\mathbf{f}^1$ is derived by filtering the initial array $\mathbf{f}^0$ with the filter $\mathbf{a}^p_0$, whose frequency response is $\{\hat{a}^p_0[n]\}$.

Proposition 4.2. *The frequency response of the filter $\mathbf{a}^p_0$ for splines of order p is*

$$\hat{a}^p_0[n] = 3^{-p}\left(1+2\cos\frac{2\pi n}{3N}\right)^p\,\frac{\tilde{u}^p_1[n]}{u^p[n]}, \quad n = 0,...,3N-1,$$

where the characteristic sequence $\tilde{u}^p_1[n]$ is defined in Eq. (4.1).

Proof. Denote $A[n] \triangleq u^p[n] + \upsilon^p_1[n] + \upsilon^p_{-1}[n]$. Then, $\hat{a}^p_0[n] = A[n]/u^p[n]$. By combining Eqs. (2.10) and (4.3), we get

$$A[n] = \sum_{l\in\mathbb{Z}}\left(1+e^{2\pi il/3}+e^{-2\pi il/3}\right)\left(\frac{\sin\pi\,(n/N+l)}{\pi\,(n/N+l)}\right)^p$$

$$= \sum_{l\in\mathbb{Z}} \left(1+2\cos\frac{2\pi l}{3}\right)\left(\frac{\sin\pi\,(n/N+l)}{\pi\,(n/N+l)}\right)^p.$$

Thus, only the terms $l=3\nu,\ \nu\in\mathbb{Z}$, in the series remain

$$A[n] = 3\sum_{l\in\mathbb{Z}} \left(\frac{\sin 3\pi\,(n/3N+l)}{3\pi\,(n/3N+l)}\right)^p.$$

By using the trigonometric identity $\sin 3\alpha = \sin\alpha\,(1+2\cos 2\alpha)$, we get

$$\begin{aligned} A[n] &= 3^{1-p}\sum_{l\in\mathbb{Z}} \left(\frac{\sin\pi\,(n/3N+l)\,(1+2\cos\pi\,(2n/3N+2l)}{\pi\,(n/2N+l)}\right)^p \\ &= 3^{1-p}\left(1+2\cos\frac{2\pi n}{3N}\right)^p \sum_{l\in\mathbb{Z}} \left(\frac{\sin\pi\,(n/3N+l)}{\pi\,(n/3N+l)}\right)^p \\ &= \frac{1}{3^p}\left(1+2\cos\frac{2\pi n}{3N}\right)^p\ \tilde{u}_1^p[n]. \end{aligned}$$

□

Corollary 4.3. *The DFT of the m-th refined array of splines of order p is*
(4.6)

$$\hat{f}^m[n]_{\tilde{m}} = \hat{a}^p_{m-1}[n]\,\hat{f}^{m-1}[n]_{\widetilde{m-1}},\quad \hat{a}^p_{m-1}[n] = \frac{1}{3^p}\left(1+2\cos\frac{2\pi n}{\tilde{N}_m}\right)^p\ \frac{\tilde{u}^p_m[n]}{\tilde{u}^p_{m-1}[n]},$$

where $\tilde{u}^p_m[n]$ are defined in Eq. (4.1), $\tilde{N}_m = N\,3^{-m},\quad n=0,...,\tilde{N}_m-1$.

4.4. **Computation of periodic splines at triadic rational points.** Now we are in a position to justify the claim about splines restoration of arbitrary order by the ternary subdivision.

Theorem 4.4. *Let $S_0(t)\in {}^p\mathcal{S}$ be an N-periodic spline of order p with nodes on the grid $\{k\},\ k\in\mathbb{Z}$, whose samples are $\left\{S(k)=f^0[k]\right\},\ k\in\mathbb{Z}$. The sequence $\mathbf{f}^0 \triangleq \left\{f^0[k]\right\},\ k\in\mathbb{Z}$, is N-periodic. Then, all the subsequent subdivision steps with the triadic periodic spline insertion rule reproduce the values of this spline*

$$f^m[k] = S(k/3^m),\quad k\in\mathbb{Z},\ m=1,2,...,. \tag{4.7}$$

Proof. From the triadic insertion rule, we have $f^1[k]\triangleq S_0(k/3)$. The next subdivision step consists of spline construction $S_1(t)\in {}^p\tilde{\mathcal{S}}_1$ on the grid $\mathbf{g}^1=\{k/3\}$, such that $S_1(k/3)=f^1[k]$. Then, $f^2[k]\triangleq S_1(k/9)$. We prove that $f^2[k]=S_0(k/9)$. The subsequent relations in Eq. (4.7) are derived by a simple induction.

The array $\mathbf{f}^2$ is obtained by successive application of the filters $\mathbf{a}^p_1$ after $\mathbf{a}^p_0$ (Proposition 4.2) to the array $\mathbf{f}^0$:

$$\begin{aligned} &\hat{f}^2[n]_{\tilde{2}} = \hat{a}^p_1[n]\,\hat{f}^1[n]_{\tilde{1}} = \hat{a}^p_1[n]\,\hat{a}^p_0[n]\,\hat{f}^0[n] \\ &\quad = \frac{1}{3^{2p}}\left(1+2\cos\frac{2\pi n}{9N}\right)^p\ \frac{\tilde{u}^p_2[n]}{\tilde{u}^p_1[n]}\left(1+2\cos\frac{2\pi n}{3N}\right)^p\ \frac{\tilde{u}^p_1[n]}{u^p[n]}\ \hat{f}^0[n] = \hat{H}[n]\,\frac{\hat{f}^0[n]}{u^p[n]}, \end{aligned} \tag{4.8}$$

$$\hat{H}[n] \triangleq \frac{1}{3^{2p}}\left(1+2\cos\frac{2\pi n}{9N}\right)^p\left(1+2\cos\frac{2\pi n}{3N}\right)^p\ \tilde{u}^p_2[n]. \tag{4.9}$$

Denote, $\mathbf{s} \stackrel{\Delta}{=} \{s[k] = S_0(k/9)\}$, $k \in \mathbb{Z}$. Similarly to Eq.(4.2), the $9N$-point DFT application to $\mathbf{s}$ is given by

(4.10)
$$\hat{s}[n]_{\tilde{2}} = \sum_{k=0}^{9N-1} e^{-2\pi ink/9N} s[k] = \hat{s}_0(n) + \sum_{l=1}^{4} \left(e^{-2\pi iln/9N} \hat{s}_l[n] + e^{2\pi iln/9N} \hat{s}_{-l}[n] \right),$$

where $\hat{s}_0(n) \stackrel{\Delta}{=} \sum_{k=0}^{N-1} \omega^{-nk} S_0(k) = \hat{f}_0(n)$ and for $l = \pm 1, \pm 2, \pm 3, \pm 4$, the following relations hold:

$$\begin{aligned} \hat{s}_l[n] &\stackrel{\Delta}{=} \sum_{k=0}^{N-1} \omega^{-nk} S_0\left(k + \frac{l}{9}\right) = \sum_{k=0}^{N-1} \omega^{-nk} \frac{1}{N} \sum_{\nu=0}^{N-1} \frac{\hat{f}^0[\nu]}{u^p[\nu]} \zeta^p[\nu] \left(k + \frac{l}{9}\right) \\ &= \sum_{k=0}^{N-1} \omega^{-nk} \frac{1}{N} \sum_{\nu=0}^{N-1} \omega^{\nu k} \frac{\hat{f}^0[\nu]}{u^p[\nu]} \zeta^p[\nu] \left(\frac{l}{9}\right) = \frac{\hat{f}^0[n]}{u^p[n]} e^{2\pi iln/9N} \bar{v}_l^p[n], \qquad (4.11) \\ \bar{v}_l^p[n] &\stackrel{\Delta}{=} e^{-2\pi iln/9N} \zeta^p[n] \left(\frac{l}{9}\right) = \sum_{\nu \in \mathbb{Z}} e^{2\nu l\pi i/9} \left(\frac{\sin \pi (n/N + \nu)}{\pi (n/N + \nu)} \right)^p. \end{aligned}$$

By substituting Eq. (4.11) into Eq. (4.10), we get

$$\begin{aligned} \hat{s}[n] &= \hat{f}^0[n] \frac{u^p[n] + \sum_{l=1}^{4} \left(\bar{v}_l^p[n] + \bar{v}_{-l}^p[n] \right)}{u^p[n]} \qquad (4.12) \\ &= \frac{\hat{f}^0[n]}{u^p[n]} \sum_{\nu \in \mathbb{Z}} \left(1 + 2 \sum_{l=1}^{4} \cos \frac{2\nu l\pi}{9} \right) \left(\frac{\sin \pi (n/N + \nu)}{\pi (n/N + \nu)} \right)^p. \end{aligned}$$

The sum $1 + 2\sum_{l=1}^{4} \cos 2\nu l\pi/9 = 9$ when $\nu = 9n$ and zero otherwise. Thus,

$$\begin{aligned} &\hat{s}[n] \\ &= \frac{9\hat{f}^0[n]}{u^p[n]} \sum_{\nu \in \mathbb{Z}} \left(\frac{\sin 9\pi(n/9N + \pi\nu)}{9(n/9N + \pi\nu)} \right)^p \\ &= 9^{1-p} \left(1 + 2\cos \frac{2\pi n}{9N} \right)^p \frac{\hat{f}^0[n]}{u^p[n]} \sum_{\nu \in \mathbb{Z}} \left(\frac{\sin 3\pi(n/9N + \pi\nu)}{(n/9N + \pi\nu)} \right)^p \\ &= 9^{1-p} \left(1 + 2\cos \frac{2\pi n}{9N} \right)^p \left(1 + 2\cos \frac{2\pi n}{3N} \right)^p \frac{\hat{f}^0[n]}{u^p[n]} \sum_{\nu \in \mathbb{Z}} \left(\frac{\sin \pi(n/9N + \pi\nu)}{(n/9N + \pi\nu)} \right)^p \qquad (4.13) \\ &= 3^{-2p} \left(1 + 2\cos \frac{2\pi n}{9N} \right)^p \left(1 + 2\cos \frac{2\pi n}{3N} \right)^p \tilde{u}_2^p[n] \frac{\hat{f}^0[n]}{u^p[n]}. \end{aligned}$$

By comparing between Eq. (4.13) and Eqs. (4.8) and (4.9), we see that $\hat{f}^2[n] = \hat{s}[n]$, $n = 0, ..., 9N-1$ and consequently, $f^2[k] = S(k/9)$, $k \in \mathbb{Z}$. Repeating the above reasoning with the initial data set $\mathbf{f}^1$ instead of $\mathbf{f}^0$, we prove that $f^3[k] = S_1(k\,3^{-3})$, and so on. □

4.5. **Computation of periodic splines at triadic rational points: Practical implementation.** It follows from Theorem 4.4 that, once we know the samples $\left\{S(k) = f^0[k]\right\}$, $k \in \mathbb{Z}$, of a spline $S(t) \in {}^p\mathcal{S}$, its values $\{S(k\,3^m)\}$, $k \in \mathbb{Z}$, $m = 1, 2, ...$, are derived by m successive refinement steps of the initial data $\mathbf{f}^0$ and the filters $\mathbf{a}_0^p$, $\mathbf{a}_1^p$,...,$\mathbf{a}_{m-1}^p$, whose frequency responses are given in Eq. (4.6). This process can be described explicitly. Due to Eq. (4.6), we get

$$\hat{f}^m[n]_{\tilde{m}} = \frac{\tilde{u}_m^p[n]}{3^{mp}\,u^p[n]}\,\hat{f}^0[n]\,\prod_{l=1}^{m}\left(1 + 2\cos\frac{2\pi n}{\tilde{N}_l}\right)^p. \tag{4.14}$$

Computation of the values $S(k/3^m) = f^m[k]$ of the spline $S(t) \in {}^p\mathcal{S}$ from the samples $S(k) = f^0[k]$ is reduced to the following three steps:

(1) Apply the $N-$point DFT to the initial data $\mathbf{f}^0 = \left\{f^0[k]\right\}$ to get $\hat{f}^0[n] = \sum_{k=0}^{N-1}\omega^{-kn}\,f^0[k]$.
(2) Derive $\hat{f}^m[n]_{\tilde{m}}$ from Eq. (4.14) bearing in mind that $u^p[n]$ and $\hat{f}^0[n]$ are $N-$periodic sequences, while $\tilde{u}_m^p[n]$, which are calculated according to Proposition 4.1, is 3^mN-periodic.
(3) Apply the 3^mN-point IDFT to the sequence $\hat{\mathbf{f}}^m = \left\{\hat{f}^m[n]_{\tilde{m}}\right\}$:

$$S(k/3^m) = f^m[k] = \frac{1}{3^mN}\sum_{n=0}^{3^mN-1} e^{-2\pi ikn/3^mN}\,\hat{f}^m[n]_{\tilde{m}}. \tag{4.15}$$

4.6. **Two-dimensional spline subdivision.** The subdivision schemes, which provide intermediate values for 1D splines, are extended to 2D cases in a natural way. A two-dimensional N-periodic spline $S(x,y) \stackrel{\Delta}{=} \sum_{k,n=0}^{N-1} s[k,n]\,B^p(x-k)\,B^q(y-n)$ from the space ${}^{p,q}\mathcal{S}$ is a 1D spline of order p with respect to x when the variable y is fixed, and a 1D spline of order q with respect to y when the variable x is fixed. Therefore, once the grid samples of the spline $\{S(k,n)\}$, $k,n = 0, ..., N-1$, are given, we can first apply either a binary (for this $p = 2r$) or a ternary 1D subdivision scheme to columns of the array $\{S(k,n)\}$, thus producing one of the two arrays $\mathbf{s}_m^P = \{S(k/P^m, n)\}$, $k = 0, ..., P^m\,N-1$, $n = 0, ..., N-1$, $P = 2$ or 3. The next step applies the subdivision algorithm to rows of the array $\mathbf{s}_m^P$, $P = 2$ or $P = 3$, thus producing one of the following four arrays:

$$\left\{S(k/P^m, n/Q^l)\right\},\ k = 0, ..., P^m\,N-1,\ n = 0, ..., Q^l\,N-1,\ P = 2 \text{ or } 3,\ Q = 2 \text{ or } 3,\ m, n \in \mathbb{N}.$$

We emphasize that a spline $S(x,y)$ can have different orders with respect to x and y. The subdivision algorithms and their depth can be different for columns and rows. In a MATLAB implementation, calculations of periodic splines are accelerated because basic operations such as the fast Fourier transforms, multiplications and divisions are applicable to the whole array rather than to separate columns and rows.

5. Experiments on upsampling of signals and images

Upsampling of discrete-time signals and digital images is an obvious application for the 1D and 2D spline subdivision.

5.1. **Upsampling of discrete-time signals.** If a signal $\mathbf{x} = \{x[k]\}$, $k = 0, ..., N-1$, $N = 2^j$, consists of samples of a smooth function $x[k] = f(k/T)$, then the subdivision techniques described in Sections 3 (Eq. (3.13)) and 4 (Eq. (4.14)) enable us to approximate the function on the intermediate points even if the grid $\{k/T\}$ is sparse. When the samples are affected by noise, then smoothing splines do a good restoration job.

Remark 5.1. If the length L of a signal $\mathbf{x} = \{x[k]\}$ to be upsampled is not a power of 2, then in order to apply the above subdivision schemes, it should be symmetrically expanded to length $N = 2^j > L$. The upsampling result should be shrunk accordingly. The same consideration is applied to processing digital images.

Example: Restoration of a noised signal. In this example, the original signal is a fragment of the *chirp* function $f(t) = \sin(1/t)$, where $t \in [0.071, 0.971]$. This fragment is displayed in Fig. 5.1. It oscillates with a variable frequency.

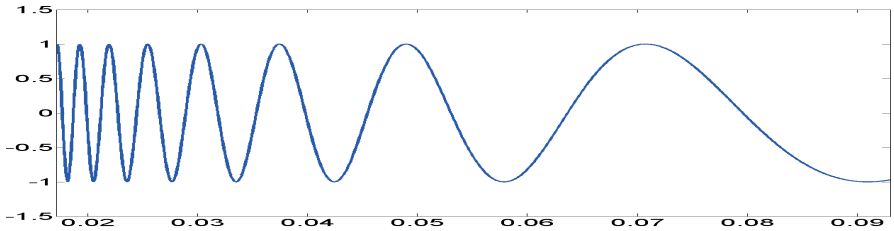

Figure 5.1. The *chirp* function $f(t) = \sin(1/t)$

In the first experiment, the data contains 128 equidistant samples of the function, which are affected by white noise with STD=0.35. This data was upsampled at ratio of 1:8 by a binary subdivision with smoothing splines of orders 4, 8 and 12, where the results are displayed in the top, middle and bottom, respectively, of the left side of Fig. 5.2. The regularization parameter ρ is derived automatically from Eq. (2.24). In the second experiment, the data was decimated by a factor of 2, thus, the initial data consisted of 64 noised samples. The data was upsampled at the ratio of 1:16 by the application of a subdivision with smoothing splines of orders 4, 8 and 12. The results are displayed in the right side of Fig. 5.2.

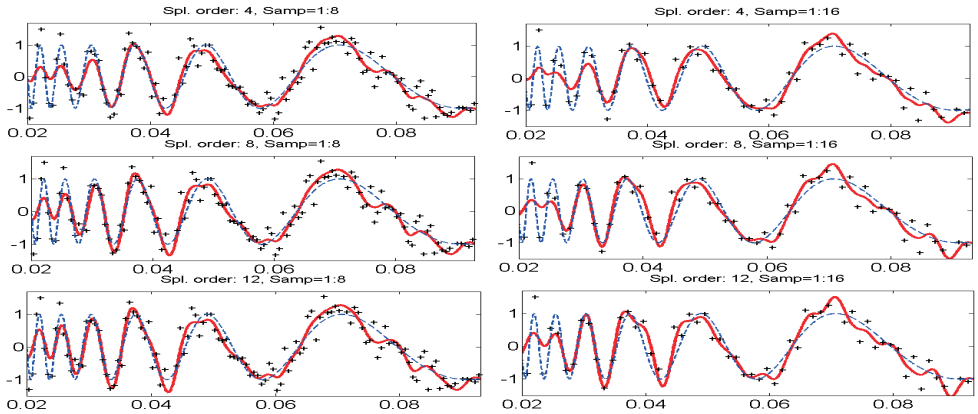

FIGURE 5.2. Left: restoration of the function $f(t) = \sin(1/t)$ from 128 noised samples by smoothing splines of order 4 (top), 8 (middle) and 12 (bottom). Right: restoration from 64 samples. Dotted line denotes the original function, "pluses" denote the available data. Solid lines denote the restored splines

We observe that, in spite of the presence of strong noise and sparse sampling, the original signal was satisfactorily restored. Note that order 4 (cubic) splines best restore the low-frequency part of the signal, while splines of 12th order restore well the high-frequency region.

5.2. **Upsampling of digital images.** Upsampling of an image using 2D interpolating splines increases its resolution. To achieve this, the image pixels are treated as grid samples of a 2D spline and the initial data array is upsampled by the spline's values in internal points, which are derived by the application of either binary (Eq. (3.13)) or ternary (Eq. (4.14)) subdivision as described in Sections 3.4 and 4.5, respectively. The 2D subdivision is outlined in Section 4.6. When pixels of the image are affected by noise, the smoothing splines provide a good approximation.

We illustrate the performance of the spline subdivision schemes by a few experiments with the benchmark images "Lena" and "Barbara", which are 512×512 pixels arrays denoted by $\mathbf{L}$ and $\mathbf{B}$, respectively.

The proximity between an approximated image $\tilde{\mathbf{L}}$ and the original image $\mathbf{L}$ is evaluated visually and by the Peak-Signal-to-Noise ratio (PSNR)

$$PSNR \triangleq 10 \log_{10} \left(\frac{M\, 255^2}{\sum_{k=1}^{M} (x_k - \tilde{x}_k)^2} \right) \; dB$$

where M is the number of pixels in the image (in our experiments, $M = 512^2$), $\{x_k\}_{k=1}^{M}$ are the original pixels of the image $\mathbf{L}$ and $\{\tilde{x}_k\}_{k=1}^{M}$ are the pixels of the image $\tilde{\mathbf{L}}$.

Example 1: "Lena" is restored from decimated arrays. In this example, the "Lena" image is restored after it was decimated by ratios of 2:1 and 4:1 to generate the data arrays $\mathbf{d}_2$ of size 256×256 and $\mathbf{d}_4$ of size 128×128. The low-pass anti-aliasing filtering was not applied to the decimated arrays. The data arrays $\mathbf{d}_s,\ s = 2, 4$ were interpolated by the even-order splines $S_s^{2r}(x, y),\ s = 2, 4$, that is $S_s^{2r}(k, n) = d_s[k, n]$. Then, the original array was restored by the splines values $L(k, n) \approx S_2^{2r}(k/2, n/2)$ and $L(k, n) \approx S_4^{2r}(k/4, n/4)$, $k, n, = 0, , , , , 511$.

The best PSNR was achieved by using subdivision with cubic splines. Figure 5.3 displays the results of this restoration. We observe that the restoration from the array $\mathbf{d}_2$ is quite satisfactory (PSNR=33.28), while the restoration from the array $\mathbf{d}_4$ is somewhat blurred (PSNR=27.25).

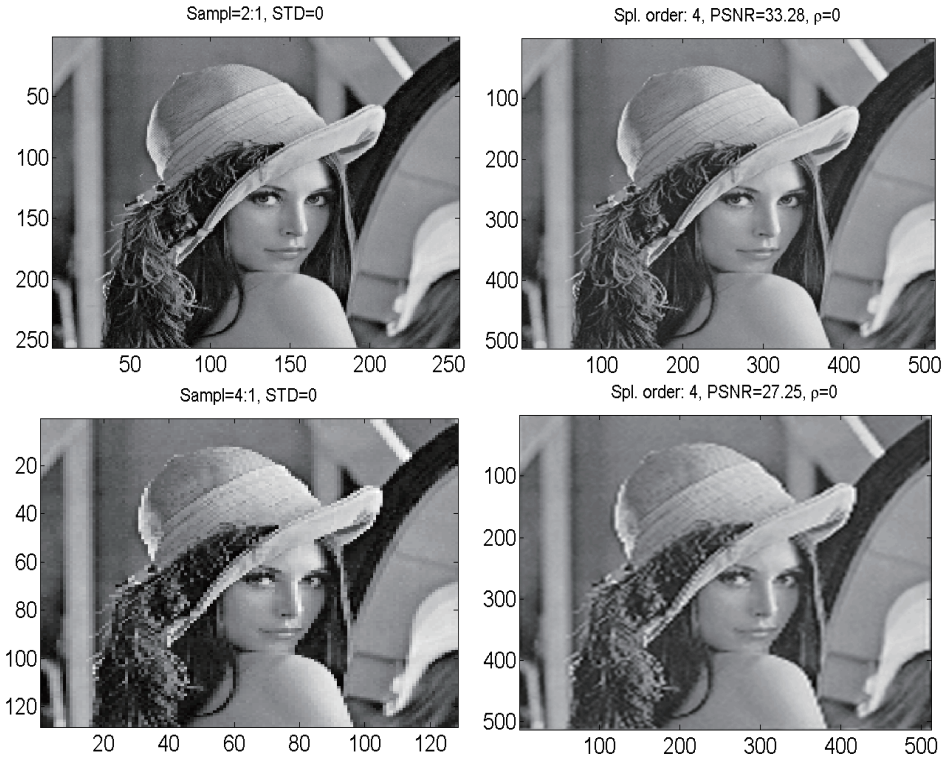

FIGURE 5.3. Left: Decimated data arrays. Top: $\mathbf{d}_2$, bottom $\mathbf{d}_4$. Right: The "Lena" image restored by the application of interpolating cubic splines subdivision from $\mathbf{d}_2$ (top) and $\mathbf{d}_4$ (bottom)

Example 2: "Lena" restoration from noised decimated arrays. In this example, the "Lena" image was decimated by factors of 2:1 and 4:1 to generate the data arrays $\mathbf{d}_2$ of size 256×256 and $\mathbf{d}_4$ of size 128×128, respectively. Then, the arrays were corrupted by a moderate Gaussian noise with STD=10. The data arrays $\mathbf{d}_s$, $s = 2, 4$, were approximated by the even-order smoothing splines $S_{\rho,s}^{2r}(x, y),\ s = 2, 4$, such that $S_{\rho,s}^{2r}(k, n) \approx d_s[k, n]$, where the optimal values of the parameter ρ were derived from Eq. (2.31). Then, the original array was restored by the splines

values $L(k,n) \approx S^{2r}_{\rho,2}(k/2, n/2)$ and $L(k,n) \approx S^{2r}_{\rho,4}(k/4, n/4)$, $k, n, = 0, \ldots, 511$. As before, the best PSNR was produced by a subdivision with cubic splines. Figure 5.4 displays the results of this restoration. We observe that noise is suppressed in the restored images. Restoration from the array $\mathbf{d}_2$ produces a satisfactory quality (PSNR=29.19), while the restoration from the array $\mathbf{d}_4$ is blurred (PSNR=26.01).

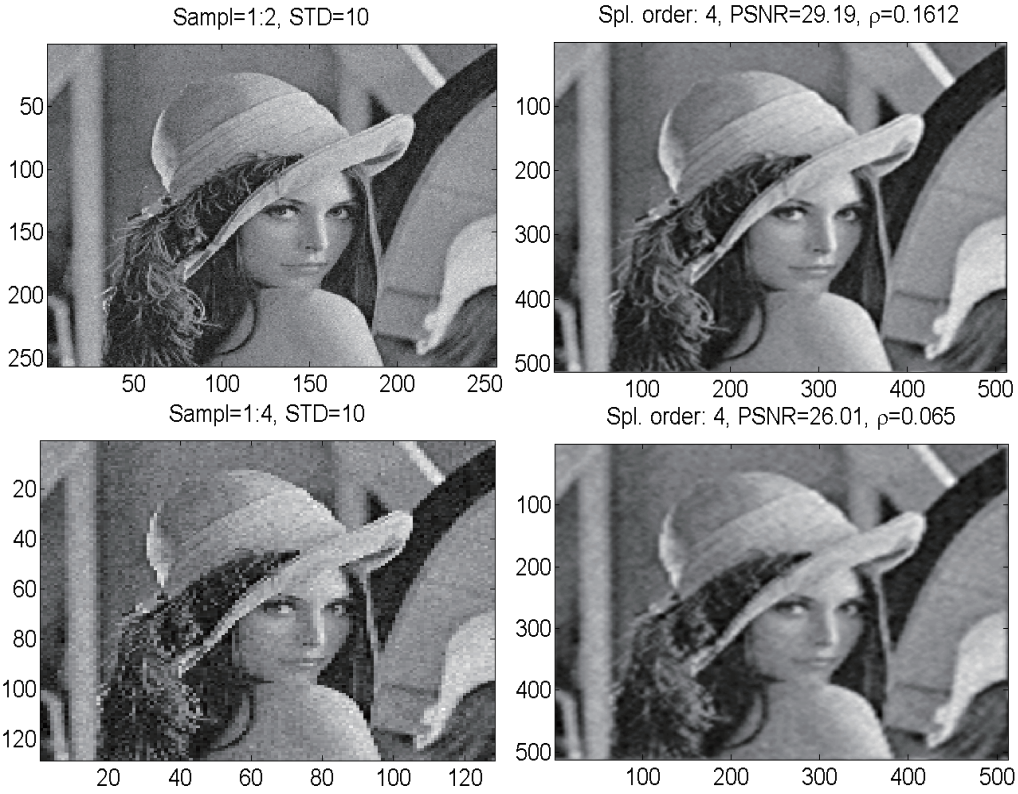

FIGURE 5.4. Left: Decimated noised images. Top: $\mathbf{d}_2$, bottom $\mathbf{d}_4$ data arrays. Right: The "Lena" image restored by the binary subdivision using the cubic smoothing splines from $\mathbf{d}_2$ (top) and from $\mathbf{d}_4$ (bottom)

Example 3: Upsampling the "Barbara" image. In this example, we upsample the "Barbara" image of size 512×512. It is given by the array $\mathbf{B}$ of pixels. We used the 2D spline $S^{7,8}(x,y)$,, which interpolates the initial data, that is $S^{7,8}(k,n) = B[k,n]$. The spline $S^{7,8}(x,y)$ is of order 7 in the vertical direction and of order 8 in the horizontal direction. By the application of 3 steps of the ternary subdivision in the vertical direction and 4 steps of the binary subdivision in the horizontal direction, we generate the array $\mathbf{S} \stackrel{\Delta}{=} \left\{S^{7,8}(k/27, n/16)\right\}$, where $k = 0, \ldots, 13823$ and $n = 0, \ldots, 8191$. Thus, the array $\mathbf{S}$ is upsampled at rate 1:27 in the vertical direction and at rate of 1:16 in the horizontal direction. The array $\mathbf{S}$ is used for the upsampled

image. The results are displayed in Fig. 5.5. We see that upsampling significantly increases the image resolution.

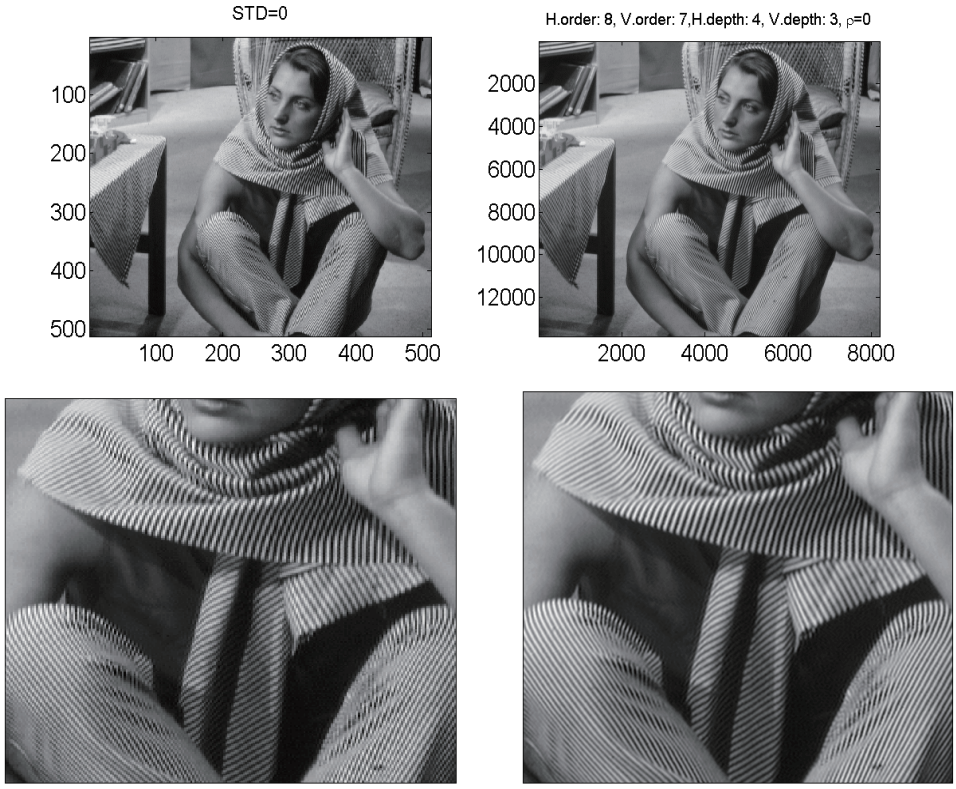

FIGURE 5.5. Left: The original "Barbara" image in two formats. Top left: The whole image. Bottom left: A fragment of the image. Right: The upsampled image after the application of the interpolating splines $S^{7,8}(x,y)$ using three steps of the ternary subdivision in the vertical direction and four steps of the binary subdivision in the horizontal direction

Example 4: Upsampling the "Barbara" image that was corrupted by noise. In this example, the pixels array $\mathbf{B}$ is corrupted by a moderate Gaussian noise with STD=10. The image was upsampled by using the 2D bicubic smoothing spline $S_\rho^{4,4}(x,y)$, which approximates the original noised data, by $S_\rho^{4,4}(k,n) \approx B[k,n]$. The optimal value of the parameter ρ was derived from Eq. (2.31). By the application of two steps of the ternary subdivision in both direction, we generated the array $\mathbf{S}_\rho \stackrel{\Delta}{=} \left\{S_\rho^{4,4}(k/9, n/9)\right\}$, $k,n = 0,\ldots,4607$. Thus, the array $\mathbf{S}_\rho$ is upsampled at rate of 1:9 in the vertical and horizontal directions. The array $\mathbf{S}_\rho$ is used as the upsampled image. The upsampled result is displayed in Fig. 5.6. We observe that the upsampling suppressed the noise while increasing the image resolution.

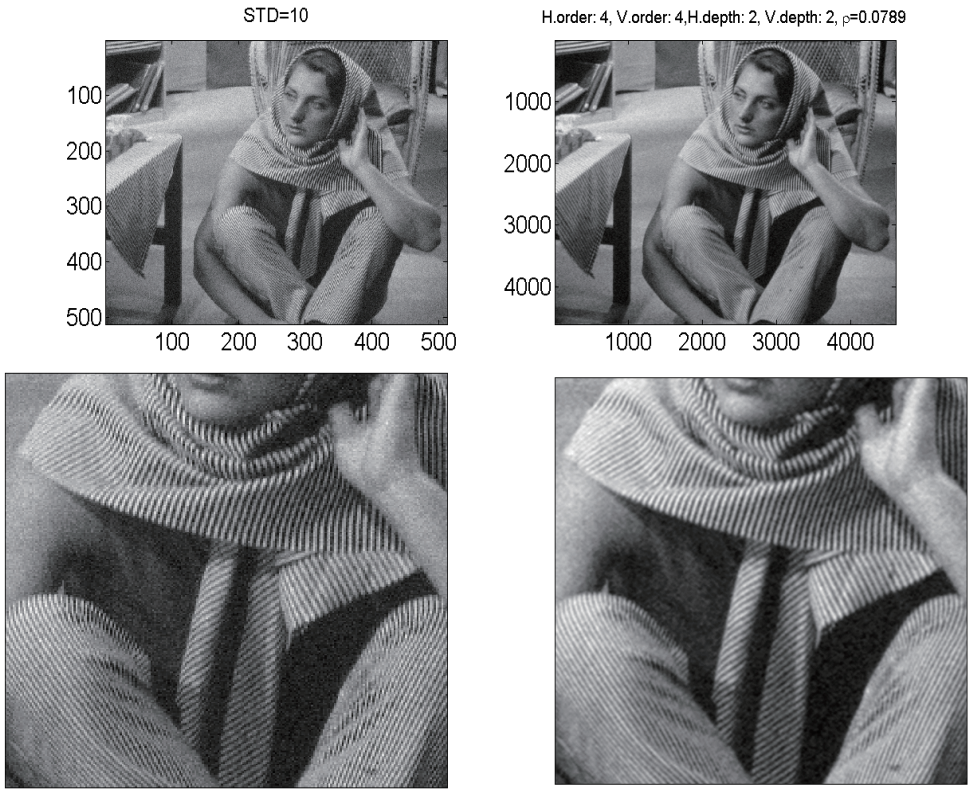

FIGURE 5.6. Left: The noised "Barbara" image in two formats. Top left: The original image. Bottom left: A fragment from the image. Right: The upsampled image by using two steps of the ternary subdivision of the the smoothing splines $S_\rho^{4,4}(x, y)$ in each direction.

Comments. The above examples demonstrate that the parameterized smoothing splines, where the regularization parameter ρ is derived automatically from Eqs. (2.24) and (2.31), efficiently suppress broad-band noise. Their mode of operation on non-decimated signals and images consists of an adaptive low-pass filtering of the input data. The filters pass-band, which are determined by the parameter ρ, depend on the signal-to-noise ratio of the available data. Suppression of strong noise is achieved by narrowing the pass-band. A side effect is that fine details of the objects become blurred. A possible way to retain fine detail in the image while suppressing noise is by the application of wavelet transforms followed by adaptive thresholding of the transform coefficients [7–9]. Another approach is to use different ρ values in different frequency domains of images. This approach, which is based on utilizing spline wavelet packets, is discussed in [5].

5.3. **The Prolate Spheroidal Wave Functions.** We now use the Prolate Spheroidal Wave Functions (PSWFs) for rate change and compare its performance to splines. In this section, we review the required material for the PSWFs that first appeared in [21].
Given a positive number c, the operator $F_c : L^2[-1,1] \to L^2[-1,1]$ is defined such that

$$F_c[\psi](x) = \int_{-1}^{1} \psi(t) e^{icxt} dt. \tag{5.1}$$

Since F_c is compact, it has a discrete set of eigenvalues $\lambda_0, \lambda_1, \ldots, \lambda_n, \ldots$. Assume that they are ordered in a non-increasing order. Let ψ_n be the eigenfunction that corresponds to λ_n. For all integer $n \geq 0$ and for all real $-1 \leq x \leq 1$, $\lambda_n \psi_n(x) = \int_{-1}^{1} \psi_n(t) e^{icxt} dt$ holds.

We assume that the eigenvectors are normalized to length 1, that is $\|\psi_n\|_{L^2[-1,1]} = 1$ (as in [16, 17, 22]). Theorem 5.2 describes the eigenvalues and the eigenfunctions of F_c.

Theorem 5.2 ([21])**.** *Suppose that $c > 0$ is a real number and the operator F_c is defined by Eq. (5.1). Then, the eigenfunctions $\psi_0, \psi_1, \ldots$ of F_c are purely real, orthonormal and complete in $L^2[-1,1]$. The even-numbered functions are even and, the odd-numbered ones are odd. Each function ψ_n has exactly n simple roots in $(-1,1)$. All the eigenvalues λ_n of F_c are non-zero and simple. The even-numbered ones are purely real and the odd-numbered ones are purely imaginary. In particular, $\lambda_n = i^n |\lambda_n|$.*

The operator $Q_c = \frac{c}{2\pi} F_c^* F_c$ has the same eigenfunctions as F_c and $Q_c[\psi](x) = \frac{1}{\pi} \int_{-1}^{1} \frac{\sin(c(x-t))}{x-t} \psi(t) dt$ where $Q_c[\psi]$ can be thought of as the output from a low pass filter and its eigenvalues are $\mu_n = |\lambda_n|^2$. This intuitively links between PSWFs and band limited functions in addition to being the eigenfunctions of the Fourier transform. The eigenvalues equation of Q_c is given by:

$$\int_{-1}^{1} \psi_n(x) \frac{\sin c(t-x)}{\pi(t-x)} dx = \mu_n \psi_n(t). \tag{5.2}$$

The solutions of Eq. (5.2) are denoted by $\psi_0(x), \psi_1(x), \psi_2(x), \ldots$ with the corresponding eigenvalues $\mu_0, \mu_1, \mu_2 \ldots$. The eigenvalues are ordered such that $\mu_0 > \mu_1 > \mu_2 \ldots$. Note that the PSWFs are the eigenfunctions of an ideal low pass filter operator and they form a basis for all bandlimited functions. We will use their basis property in the interpolation procedure. The ability of the PSWFs to approximate accurately bandlimited functions has been recently investigated in [20].

Figure 5.7 shows the fast decay of the eigenvalues of F_c (in absolute value).

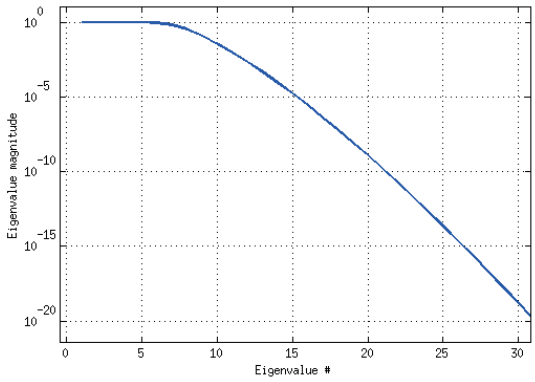

FIGURE 5.7. Eigenvalues of F_c in absolute value for $c = 10$

5.3.1. *Problem Setup.* Assume we are given a set of points $\{x_i\}_{i=1}^N$ on the interval $[-1, 1]$ taken from a bandlimited function $f(x)$ with bandwidth c and an additional point z. We want to compute the weights $\{h_i\}_{i=1}^N$ that approximate $f(z)$ such that $\tilde{f}(z) = \sum_{i=1}^N h_i f(x_i)$. Moreover, we are looking for a solution that is independent of the actual value of the function $f(x)$ so it can be applied to any bandlimited function with bandwidth c. The weights computation can be done by approximating a basis for the bandlimited functions. If the basis functions are approximated then we can find weights applicable to all the bandlimited functions (bandwidth c). Given bandwidth c, a set of points $\{x_i\}_{i=1}^N$ and a point z, we can solve the following least-squares (LS) problem by minimizing $\epsilon = \|e^{ic\omega z} - \sum_{i=1}^N h_i e^{ic\omega x_i}\|_2^2$ to compute the weights $\{h_i\}_{i=1}^N$.

Complex exponents are taken as basis functions since they are the eigenfunctions of Linear-Time-Invariant (LTI) systems. By computing the gradient of $\epsilon(\mathbf{h})$ and setting it to zero, we get the following set of linear equations: $\frac{\partial \epsilon}{\partial h_m} = \langle e^{ic\omega z} - \sum_{i=1}^N h_i e^{ic\omega x_i}, h_m e^{ic\omega x_m} \rangle = 0$, $\langle e^{ic\omega z}, e^{ic\omega x_m} \rangle - \sum_{i=1}^N h_i \langle e^{ic\omega x_i}, e^{ic\omega x_m} \rangle = 0$ to obtain for $m = 1, ..., N$

$$\frac{\sin c(z - x_m)}{c(z - x_m)} - \sum_{i=1}^{N} h_i \frac{\sin c(x_i - x_m)}{c(x_i - x_m)} = 0. \tag{5.3}$$

Equation (5.3) represents an $N \times N$ system of equations $\mathbf{Ah} = \mathbf{b}$ where $a_{mn} = \frac{\sin c(x_m - x_n)}{c(x_m - x_n)}$ and $b_n = \frac{\sin c(z - x_n)}{c(z - x_n)}$. This system consists of sinc functions, which are known to be optimal for the interpolation of bandlimited functions. In practice, however, this method (Eq. 5.3) is far from being optimal due to the rapid growth of the condition number of $\mathbf{A}$. Hence, even for small number of samples and a low frequency signal the condition number is large.

5.3.2. *Interpolation using PSWFs.* Since $f(x)$ is bandlimited it can be represented as a linear combination of PSWFs $f(x) = c_1\psi_1(x) + c_2\psi_2(x) + \ldots + c_n\psi_n(x) + \ldots$. It takes a series of approximated length $M = O(c + log(c))$ to achieve a good approximation of the order λ_{M+1} [20]. The eigenvalues decay as a function of c

such that the first $c+log(c)$ eigenvalues are of order 1 and the others are very close to zero (Fig. 5.7). Since f can be approximated with PSWFs, it is possible to use the same basis approach as in Section 5.3.1 and interpolates the values of the PSWFs by finding the weights. It is known that sinc functions are optimal. Equation 5.3 can be reformulated in terms of PSWFs by maintaining the theoretical optimality. The matrices $\mathbf{A} = \{a_{mn}\} = \frac{\sin c(x_m - x_n)}{c(x_m - x_n)}$ and $\mathbf{b} = \{b_n\} = \frac{\sin c(z - x_n)}{c(z - x_n)}$ can be factorized using a new matrix $\mathbf{C}$, which is not necessarily square, such that $\mathbf{A} = \mathbf{C^T C}$ and $\mathbf{b} = \mathbf{C^T \tilde{b}}$. By using the identity $\frac{\sin c(x_m - x_n)}{c(x_m - x_n)} = \sum_j |\lambda_j|^2 \psi_j^c(x_m)\psi_j^c(x_n)$, we get that the matrix $\mathbf{C}$ is $c_{mn} = |\lambda_m|\psi_m(x_n)$. By rewriting Eq. (5.3) in terms of the new matrix, we get $\mathbf{C^T C h} = \mathbf{C^T \tilde{b}}$ which is the weighted LS solution of

$$\mathbf{C h} = \tilde{\mathbf{b}} \tag{5.4}$$

where $\tilde{b}_n = \psi_n(x_n)$. Explicitly, Eq. 5.4 can be written as:

$$\begin{aligned}
|\lambda_1|\psi_1(z) &= c_1|\lambda_1|\psi_1(x_1) + ... + c_N|\lambda_1|\psi_1(x_N) \\
|\lambda_2|\psi_2(z) &= c_1|\lambda_2|\psi_2(x_1) + ... + c_N|\lambda_2|\psi_2(x_N) \\
&\vdots \\
|\lambda_M|\psi_M(z) &= c_1|\lambda_M|\psi_M(x_1) + ... + c_N|\lambda_M|\psi_M(x_N).
\end{aligned}$$

Equation 5.4 has the same (least-squares) solution as Eq. (5.3). Its condition number is exactly the square root of the matrix in Eq. (5.3). It is shown in [19] that the obtained solution of Eq. (5.4) is very accurate despite the large condition number. In short, given the SVD $\mathbf{U\Sigma V^T}$ of $\mathbf{C}$, then, the singular values of $\mathbf{C}$ are almost identical to the absolute values of the eigenvalues λ_i such that $\sigma_i(\mathbf{C}) = \mathcal{O}(|\lambda_i|)$ (see Fig. 5.8) leading to numerically stable equations as the left hand side is proportional to the right hand side which is dominated by $|\lambda_i|$. This "balance" provides an accurate numerical solution. A more rigorous analysis is also required to analyze the matrix $\mathbf{U}$ of the SVD as it can theoretically reorder the equations. A complete analysis appears in [19].

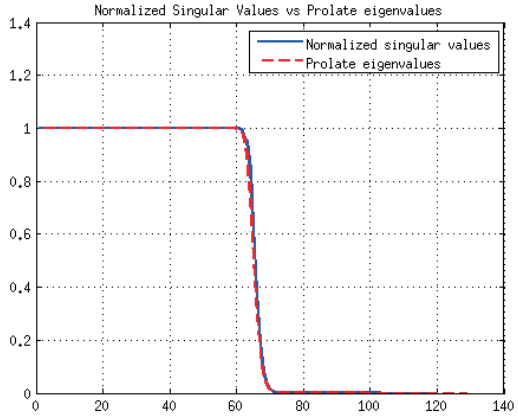

FIGURE 5.8. The singular values of $\mathbf{C}$ vs $|\lambda_i|$

Figure 5.8 shows the singular values of the matrix $\mathbf{C}$ with respect to the PSWF's eigenvalues which indicate that the equation can be solved accurately despite the large condition number.

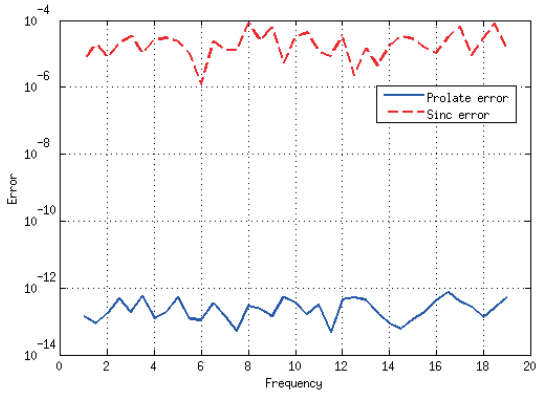

FIGURE 5.9. Error comparison between Sinc and Prolate methods

Equation 5.4 was tested on a bandlimited function $f(x) = \cos(2\pi f x)$ where the number of samples is $N = 2f$. An even number of equispaced samples were taken on the interval $[-1, 1]$ and the interpolation goal was to reconstruct f at $x = 0$. Figure 5.9 compares between the numerical error obtained using sinc functions with the error obtained using PSWFs under identical conditions. Clearly, the numerical error obtained using PSWFs is smaller by a factor 10^8.

The interpolation-based PSWF is achieved by the application of the interpolation scheme to each dimension separately. By assuming that both dimensions have the same bandwidth (same c is used) then the weights can be computed only once.

We now compare between the performances (three criteria) of splines of order 8 and PSWFs on digital images: visual quality (see Fig. 5.10), achieved PSNR and computational time (see both in Table 5.1).

We see that the splines produce better quality with less artifacts although the achieved PSNR (Table 5.1) are very similar.

Upsampling	PSWF PSNR	Spline PSNR	PSWF Time [sec]	Spline Time [sec]
2	28.7	29.2	24	0.05
4	24.7	24.4	41	0.2
8	22.1	21.8	80	0.8
16	20.5	20	150	3.4

TABLE 5.1. Performance comparison on the achieved PSNRs and on the processing time between splines of order 8 and prolates for the usampling by factor 2, 4, 8 and 16 of the source image in Fig. 5.10.

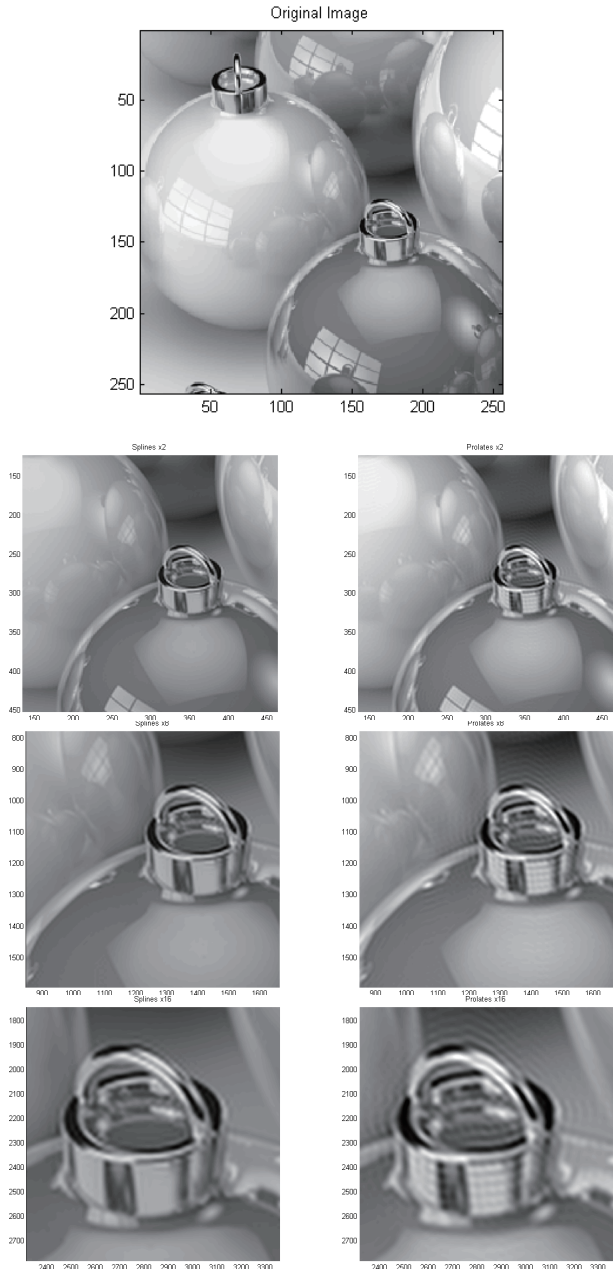

FIGURE 5.10. Comparison between the upsampling performance by factors 2,8 and 16 of spline of order 8 (left column) and prolate with $c = 280$ (right column)

Conclusions

The advantages of the smoothing splines is in the simplicity of their implementation and in their automatic adaptation to the available data.

The subdivision schemes in this paper, which reduce splines computation of any order, are built from one pass application of the forward FFT and from one pass application of the inverse FFT. Additional adaptation abilities stem from the freedom of choice of splines involved in the upsampling process. Surely, the field of applications of the subdivision algorithms is not confined to upsampling signals and images. The most common application is the geometric design/modeling (see [12], for example).

Acknowledgement

The authors would like to thank Andrei Osipov and Vladimir Rokhlin from Yale University and Yoel Shkolnisky from Tel-Aviv University for fruitful discussions and for providing part of the PSWFs code.

References

[1] J. H. Ahlberg and E. N. Nilson and J. L. Walsh, *The Theory of splines and their Applications*, Acad. Press, New York, 1967.

[2] A. Averbuch and V. Zheludev, *Spline-based deconvolution* Signal Processing **89** (2009), 1782–1797.

[3] A. Averbuch and V. Zheludev and G. Fatakhov and E. Yakubov, *A ternary interpolatory subdivision schemes originated from splines*, International Journal of Wavelets, Multiresolution and Information Processing **9** (2011), 611–633.

[4] A. Averbuch and V. Zheludev and M. Khazanovsky, *Deconvolution by Matching Pursuit using spline wavelet packets dictionaries*, Applied and Comp. Harmonic Analysis **31** (2011), 98–124.

[5] A. Averbuch and V. Zheludev and P. Neittaanmäki and J. Koren, *Block based deconvolution algorithm using spline wavelet packets*, Journal of Mathematical Imaging and Vision **38** (2010), 197–225.

[6] M. J. Bastiaans, *Gabor expansion and the Zak transform for continuous-time and discrete-time signals*, in: Signal and Image Representation in Combined Spaces, Wavelet Anal. Appl., 7, Y. Y. Zeevi and R. Coifman (eds.), Academic Press, San Diego, CA, 1998, pp. 23–69.

[7] S. G. Chang and B. Yu and M. Vetterli, *Adaptive Wavelet Thresholding for Image Denoising and Compression*, IEEE Trans. on Image Proc. **9** (2000), 1532–1546.

[8] D. Donoho and I. Johnstone, *Adaptating to unknown smoothness via wavelet shrinkage*, J. Amer. Stat. Soc. **90/432** (1994), 1200–1224.

[9] D. Donoho and I. Johnstone, *Ideal spatial adaptation via wavelet shrinkage*, Biometrica **81** (1994), 425–455.

[10] N. Dyn, *Tutorials on Multiresolution in Geometric Modelling*, *Chapter* Analysis of convergence and smoothness by the formalism of Laurent polynomials, A. Iske and E. Quak and M.S. Floater (eds.), Springer, 2002, pp. 51–68.

[11] N. Dyn and J. A. Gregory and D. Levin, Analysis of uniform binary subdivision schemes for curve design, *Constr. Approx.* **7** (1991), 127–147.

[12] N. Dyn and D. Levin, *Subdivision schemes in geometric modelling*, Acta Numerica **11** (2002), 73–144.

[13] J. C. Holladay, *Smoothest curve approximation*, Math. Tables Aids Comput. **11** (1957), 233–243.

[14] K. P. Ko, and B-G Lee, and G. J. Yoon, *A ternary 4-point approximating subdivision scheme*, Applied Mathematics and Computation **190** (2007), 1563–1573.

[15] M. Hassan, I. Ivrissimitzis, N. Dodgson, M. Sabin, *An interpolating 4-point C^2 ternary stationary subdivision scheme*, CAGD **19** (2002), 1–18.
[16] A. Osipov and V. Rokhlin and H. Xiao, *Prolate Spheroidal Wave Functions of Order Zero*, Springer, 2013.
[17] V. Rokhlin and H. Xiao, *Approximate formulae for certain prolate spheroidal wave functions valid for large value of both order and band limit*, Applied and Computational Harmonic Analysis **22** (2007), 105–123.
[18] I. J. Schoenberg, *Spline functions and the problem of graduation*, Proc. Nat. Acad. Sci. USA **52** (1964), 947–950.
[19] G. Shabat and Y. Shkolnisky and A. Averbuch, *High precision interpolation of band limited functions*, Private communication.
[20] Y. Shkolnisky and M. Tygert and V. Rokhlin, *Approximation of bandlimited functions*, Applied and Computational Harmonic Analysis **21** (2006), 413–420.
[21] D. Slepian and H. O. Pollak, *Prolate spheroidal wave functions, Fourier analysis, and uncertainty - I*, Bell System Techincal J. **22** (1961), 43–63.
[22] H. Xiao and V. Rokhlin and N. Yarvin, *Prolate spheroidal wave functions, quadrature and interpolation*, Inverse Problems **17** (2001), 805–828.
[23] J. Zak, *Finite translations in solid-state physics*, Phys. Rev. Lett. **19** (1967), 1385–1387.
[24] V. A. Zheludev, *Periodic splines, harmonic analysis and wavelets*, in: Signal and Image Representation in Combined Spaces, Wavelet Anal. Appl., 7, Y. Y. Zeevi and R. Coifman (eds.), Academic Press, San Diego, CA, 1998, pp. 477–509.
[25] V. A. Zheludev, *Interpolatory subdivision schemes with infinite masks originated from splines*, Advances in Comp. Math. **25** (2006), 475–506.

Manuscript received April 17 2016
revised June 16 2016

Amir Z. Averbuch
School of Computer Science, Tel Aviv University, Tel Aviv 69978, Israel
E-mail address: amir@math.tau.ac.il

Pekka Neittaanmäki
Department of Mathematical Information Technology, P.O. Box 35 (Agora), University of Jyväskylä, Finland
E-mail address: pn@jyu.fi

Gil Shabat
School of Computer Science, Tel Aviv University, Tel Aviv 69978, Israel
E-mail address: gilgil.s@gmail.com

Valery A. Zheludev
School of Computer Science, Tel Aviv University, Tel Aviv 69978, Israel
E-mail address: zhel@post.tau.ac.il